

THE HALL EFFECT ON MHD 2-FLUID UNSTEADY HEAT TRANSFER FLOW OF PLASMA IN A ROTATING SYSTEM VIA A STRAIGHT CHANNEL BETWEEN CONDUCTING PLATES

T. LINGA RAJU* and B. VENKATA RAO

Department of Engineering Mathematics, AUCE (A), Andhra University, Visakhapatnam
Andhra Pradesh, Pin code- 530003, INDIA

E-mail:tlraju45@yahoo.com

Abstract: Hall currents are used to investigate MHD unsteady two fluid flows and heat transport of plasma along a straight channel of conducting plates. In the two liquid zones, the velocity and temperature fields for the case of conducting side plates are obtained by solving the governing equations using a two-term series under the specified conditions. The distribution profiles are graphically resolved and examined. The distributions are thought to be dependent on the electron-to-total pressure ratio. The flow and heat transfer factors are also influenced by other parameters such as the Hartmann number, Hall parameter, rotation parameter, thermal conductivity and viscosity ratio.

Keywords: unsteady flow, MHD, immiscible flow, heat transfer, Hall effect, plasma, rotating frame, conducting plates.

1. Introduction

The study of MHD flow models in a variety of conditions and geometrical approach has been an important focus of research for decades in a variety of domains. It is interesting to examine the amount of heat flow and the temperature distribution pattern that heat transfer produces in channels when moving in an unsteady or steady motion, used for diverse applications in mechanical, electrical, chemical and biochemical engineering, geothermal energy extraction, and industrial problems. Oscillatory flows are also frequently employed to improve heat transfer rates in a variety of industrial processes, resulting in a significant technical shift toward efficiency. A number of scholars successfully addressed such problems using single fluid models [1-13]. The use of liquid metals as heat transfer agents and working fluids in MHD power generator and nuclear reactor technology has sparked an increased awareness in the behavior of liquid metal flows, thermal processes occurring at extremely high temperatures, and to be specific, the interaction with ionized fluids and electro-magnetic fields in a rotating environment.

The impact of the rotating component on a range of technical and industrial operations, such as channel flow and heat transfer, is important. Because the introduction of Coriolis forces in a flow field can change the entire dynamics of the flow process, it has the potential to change the mainstream flow. The presence of magneto hydrodynamic forces and Hall currents has been proven in the literature to have a significant impact on MHD channel flows in a rotating framework. Many astrophysical and geophysical problems rely on Hall currents, such as plasma flows into MHD power generator, plasma jets, and hall accelerators. Several studies on the issue have been reported in the literature due to their applications in a variety of industrial and technological sectors [14-24].

Furthermore, it is well understood that in a realistic state of affairs, fluid flows in general are unsteady/transient. This unsteadiness is responsible for a number of practical issues that emerge when working with immiscible fluids. Multi-fluid/ 2-liquid flow regimes are a significant matter of concern in the petroleum industry, geophysics, plasma physics, magneto-fluid dynamics, and other fields. In a

* To whom correspondence should be addressed

number of practical applications, it is useful to consider both immiscible fluids to be electrically conducting, especially when one is a better electric conductor than the other. Fluids having low electrical conductivity are significant for reducing power consumption while pumping fluid in MHD pumps and flow meters. Due to the significance of such studies, several investigations were extensively made and published in the literature [25-32].

Mitra [33] considered the flow of two electrically conducting liquids among two rigid parallel plates in an unsteady motion. Hasnain *et al.* [34] considered the statistical features of a three-dimensional 2-liquid plasma flow model. Umavathi *et al.* [35] solved an oscillatory Hartmann 2- liquid heat transfer flow through horizontal channel. L.Raju and S.Dhar investigated the unsteady two liquid heat transfer flow of conductive liquids within a channel under the influence of a magnetic field [36]. An MHD 2-layer unsteady heat transfer flow in a horizontal channel among parallel plates in a rotating frame of reference was investigated by L.Raju and Valli [37]. An MHD two liquid heat transfer flow across a horizontal tube was investigated by Sharma and Sharma [38]. Gireesha *et al.* [39] investigated Hall effects on a dusty nano fluid two-phase transient flow via a stretching sheet using the KVL model. Sivakamini and Govindarajan [40] explored the unsteady MHD flow of 2-immiscible liquids through a horizontal channel with chemical reaction. AbdElmaboud *et al.* [41] investigated the immiscible liquids electromagnetic flow. The influence of Hall current on an unsteady MHD 2- ionised fluid heat transfer flow inside a channel was studied by L.Raju and Gowri [42]. For the situation of non-conducting (insulating) plates, L.Raju and Venkat [43] examined an unsteady EMHD flow and heat transfer of 2 ionized liquids in a rotating system with Hall currents.

Therefore, it is important to have a look into just how Hall currents alter the outcomes of unsteady MHD two liquid plasma flows in channels /or ducts surrounded by conducting plates. Many astrophysical, geophysical problems, and laboratory environments, such as plasma flows in MHD power generators, plasma jets, and Hall accelerators, high-temperature thermal processes, and crystal growth, all rely heavily on Hall currents under the influence of an applied magnetic field.

So, Hall currents are used in this paper to investigate an MHD two liquid unsteady heat transfer flow of plasma into a straight channel in a rotating framework while the channels plates are composed of conductive materials. This theoretical research is anticipated to have some practical application in the development of the conceptual design of fusion reactors, control of hot moving liquid in metallurgical engineering applications, aerodynamic heating, plasma jets and liquid metal MHD rotating generators, MHD pumps and flow meters, Hall accelerators, etc. driven by Lorentz force, and geothermal energy extraction as well as aerospace science.

2. Formulation of the problem

An unsteady magneto hydrodynamic 2- liquid flow of ionized gases in a parallel channel between two conducting plates extending along the x and z directions, taking into account Hall currents, controlled by a uniform constant gradient $-\frac{\partial p}{\partial x}$ is studied. The fluids and plates are assumed to be rigidly rotating around the y axis normal to the plates at a uniform angular velocity $\bar{\Omega}$. The liquids are subjected to a constant magnetic field B_0 applied normal to the plates. The x axis is measured in the direction of the hydraulic pressure gradient in a plane parallel to the channel plates, not in the flow direction. Region-I and region-II refer to the upper and lower fluids in the regions: $0 \leq y \leq h_1$ and $-h_2 \leq y \leq 0$. Two immiscible electrically conducting incompressible fluids with distinct densities ρ_1, ρ_2 , viscosities μ_1, μ_2 , and electrical conductivities σ_{01}, σ_{02} , thermal conductivities K_1 and K_2 occupy in region-I and region-II. The two fluids thermal characteristics are considered stable. The channels plates are kept at the same temperature, so the temperature at the top plate is the same as that at bottom plate. Except for pressure, all physical quantities are functions of the variables y and t , with the two plates being infinitely long in the x and z axes. The two immiscible fluids interface is assumed to be flat, stress-free, and undisturbed. It is assumed that the magnetic Reynolds number is low. These assumptions along with these of the studies [14, 28, 32 and 42] are used to

formulate the governing equations of motion, current, and energy. It is also considered that $\overline{V}_i = (u_i, 0, w_i)$, $\overline{B} = (0, B_0, 0)$, $\overline{\Omega} = (0, \Omega, 0)$, $\overline{J}_i = (J_{ix}, 0, J_{iz})$, $\overline{E}_i = (E_{ix}, 0, E_{iz})$, $i = 1, 2$ in both the upper and lower regions when the plates are conducting. As a result, the following transformations are used to make the governing equations and conditions dimensionless.

$$\begin{aligned}
 i = 1, 2; \quad y_i^* &= \frac{y_i}{h_i}, \quad u_p = -\frac{\partial p}{\partial x} \left(\frac{h_i^2}{\mu_i} \right), \quad u_i^* = \frac{u_i}{u_p}, \quad w_i^* = \frac{w_i}{u_p}, \quad t^* = \frac{t \mu_i}{\rho_i h_i^2}, \quad \omega^* = \frac{\omega h_i^2 \rho_i}{\mu_i}, \\
 m_{ix} &= \frac{E_{ix}}{B_0 u_p}, \quad m_{iz} = \frac{E_{iz}}{B_0 u_p}, \quad I_{ix} = \frac{J_{ix}}{\sigma_{0i} B_0 u_p}, \quad I_{iz} = \frac{J_{iz}}{\sigma_{0i} B_0 u_p}, \quad M^2 = B_0^2 h_i^2 \left(\frac{\sigma_{0i}}{\mu_i} \right), \\
 K^2 &= \frac{h_i^2 \rho_i \Omega}{\mu_i}, \quad \alpha = \frac{\mu_1}{\mu_2}, \quad h = \frac{h_2}{h_1}, \quad \sigma_0 = \frac{\sigma_{01}}{\sigma_{02}}, \quad \sigma_1 = \frac{\sigma_{12}}{\sigma_{11}}, \quad \sigma_2 = \frac{\sigma_{22}}{\sigma_{21}}, \quad \frac{l}{1+m^2} = \frac{\sigma_{11}}{\sigma_{01}}, \\
 \frac{m}{1+m^2} &= \frac{\sigma_{21}}{\sigma_{01}}, \quad m = \frac{w_e}{\left(\frac{l}{\tau} + \frac{l}{\tau_e} \right)}, \quad \beta = \frac{K_1}{K_2}, \quad \theta_i = \frac{T_i - T_{wi}}{(u_p^2 \mu_i / K_i)}.
 \end{aligned} \tag{2.1}$$

For the two liquids $i = 1, 2$: the parameters M , m , K , h , α , σ_0 , β and θ_i denote the Hartmann number, Hall parameter, Taylor number (or rotation parameter), height ratio, viscosity ratio, electrical-conductivity ratio, thermal conductivity ratio, and temperature distributions. In addition, ω_e represents the electrons gyration frequency, τ and τ_e represent the mean collision times between electron and ion and electron and neutral particles, and t represents the time variable. When τ_e approaches infinity, the expression for Hall parameter m in Eq.(2.1) holds true for partially ionized gas and the expression is consistent with fully ionized gas.

Additionally, when the plates are formed of a conducting material and are short-circuited by an outside conductor, the induced electric current flows out of the channel. At this stage, there is no electric potential between the side plates. Also $m_{ix} = 0$ and $m_{iz} = 0$ are obtained if we take 0 (zero) electric field in the x and z directions (see [14] and [32]). As a result, when the channels plates are comprised of a conducting material, the dimensionless controlling equations of motion, current, temperature, and conditions in the two zones are (by just overlooking the asterisks):

Region-I (For motion at the upper zone)

$$\frac{\partial u_1}{\partial t} - \frac{\partial^2 u_1}{\partial y^2} + \frac{M^2 u_1}{1+m^2} + \frac{M^2 m w_1}{1+m^2} + \frac{m^2 s}{1+m^2} - l = -2K^2 w_1, \tag{2.2}$$

$$\frac{\partial w_1}{\partial t} - \frac{\partial^2 w_1}{\partial y^2} + \frac{M^2 w_1}{1+m^2} - \frac{M^2 m u_1}{1+m^2} + \frac{ms}{1+m^2} = 2K^2 u_1, \tag{2.3}$$

$$\frac{\partial \theta_1}{\partial t} = \frac{l}{P_{r1}} \frac{\partial^2 \theta_1}{\partial y^2} + \left\{ \left(\frac{\partial u_1}{\partial y} \right)^2 + \left(\frac{\partial w_1}{\partial y} \right)^2 \right\} + M^2 I_1^2, \tag{2.4}$$

$$I_{1x} = \frac{mu_1}{l+m^2} - \frac{w_1}{l+m^2} - \frac{s}{M^2} \frac{m}{l+m^2}, \quad (2.5)$$

$$I_{1z} = \frac{u_1}{l+m^2} + \frac{mw_1}{l+m^2} + \frac{s}{M^2} \left(l - \frac{m}{l+m^2} \right), \quad (2.6)$$

and $I_1^2 = I_{1x}^2 + I_{1z}^2$.

Region-II (For motion at the lower zone)

$$\frac{\partial u_2}{\partial t} - \frac{\partial^2 u_2}{\partial y^2} + \frac{\alpha\sigma_1 h^2 M^2 u_2}{l+m^2} + \frac{m\alpha\sigma_2 h^2 M^2 w_2}{l+m^2} - \left\{ l - \left(l - \frac{\sigma_0\sigma_1}{l+m^2} \right) \right\} s\alpha h^2 = -2\rho\alpha h^2 K^2 w_2, \quad (2.7)$$

$$\frac{\partial w_2}{\partial t} - \frac{\partial^2 w_2}{\partial y^2} + \frac{\alpha\sigma_1 h^2 M^2 w_2}{l+m^2} - \frac{m\alpha\sigma_2 h^2 M^2 u_2}{l+m^2} + \frac{\sigma_0\sigma_2\alpha h^2 ms}{l+m^2} = 2\rho\alpha h^2 K^2 u_2, \quad (2.8)$$

$$\frac{\partial \theta_2}{\partial t} = \frac{1}{P_{r2}} \frac{\partial^2 \theta_2}{\partial y^2} + \frac{\beta}{\alpha} \left\{ \left(\frac{\partial u_2}{\partial y} \right)^2 + \left(\frac{\partial w_2}{\partial y} \right)^2 \right\} + h^2 \sigma \beta M^2 I_2^2 \quad (2.9)$$

$$I_{2x} = \frac{m\sigma_0\sigma_2 u_2}{l+m^2} - \frac{\sigma_0\sigma_1 w_2}{l+m^2} - \frac{s\sigma_0^2\sigma_2}{M^2} \frac{m}{l+m^2} \quad (2.10)$$

$$I_{2z} = \frac{\sigma_0\sigma_1 u_2}{l+m^2} + \frac{m\sigma_0\sigma_2 w_2}{l+m^2} + \left(l - \frac{\sigma_0\sigma_1}{l+m^2} \right) \frac{s\sigma_0}{M^2}, \quad \text{and } I_2^2 = I_{2x}^2 + I_{2z}^2. \quad (2.11)$$

Conditions on the velocities are given by

$$\text{at } y = -l, \quad u_1 = 0 \text{ for } t \leq 0 \text{ and } = (\varepsilon \cos \omega t), \quad t > 0, \quad (2.12)$$

$$w_1 = 0, \quad t \leq 0 \text{ and } = (\varepsilon \cos \omega t), \quad t > 0.$$

$$\text{At } y = -l, \quad u_2 = 0 \text{ and } w_2 = 0. \quad (2.13)$$

$$\text{At the interface } y = 0: \quad u_1 = u_2, \quad w_1 = w_2, \quad \frac{\partial u_1}{\partial y} = \left(\frac{l}{\alpha h} \right) \frac{\partial u_2}{\partial y}, \quad \frac{\partial w_1}{\partial y} = \left(\frac{l}{\alpha h} \right) \frac{\partial w_2}{\partial y}. \quad (2.14)$$

The temperature conditions at the boundary and interface are determined by

$$\theta_1 = 0 \text{ at } y = l \text{ and } \theta_2 = 0 \text{ at } y = -l. \quad (2.15)$$

$$\text{At the interface } y = 0, \quad \text{we have } \theta_1 = \theta_2 \quad \text{and} \quad \frac{d\theta_1}{dy} = \frac{l}{h\beta} \frac{d\theta_2}{dy}. \quad (2.16)$$

Subscripts 1 and 2 in the preceding equations relate to liquid quantities in the upper and lower areas. The velocity components in the x and z axes of the two liquids, u_1, u_2 , and w_1, w_2 , are referred to as main and secondary velocity distributions. E_{ix}, E_{iz} and J_{ix}, J_{iz} are the components of the electric field and current densities in the x and z directions. The ratio of electron pressure to total pressure is indicated by the notation $s = pe / p$. T_1 and T_2 denote the temperatures of the two fluids, Ω is the angular velocity, C_{pi} is the specific heat at constant pressure, and the symbols, σ_{11}, σ_{12} and σ_{21}, σ_{22} signify the modified conductivities parallel and perpendicular to the direction of the electric field.

3. Solution method

With the aim of solving energy equations (2.4) and (2.9) using conditions (2.15-2.16), first of all the momentum equations (2.2, 2.3, 2.7 and 2.8) are solved for the velocity fields by conditions (2.12-2.14); thereby we obtained expressions for currents: I_{1x}, I_{1z} and I_{2x}, I_{2z} . As a consequence, it is possible to determine the temperature distribution in the two locations (θ_1, θ_2) as well as the rate of the heat transfer coefficient Nu_1 and Nu_2 at the conducting plates. This system of equations is impossible to solve in closed form because there are coupled partial differential equations. As a result, they can be determined utilizing the following pair series [Ref. 42 and 43].

$$u_1(y,t) = u_{01}(y) + (\epsilon \cos \omega t) u_{11}(y) \quad \text{and} \quad w_1(y,t) = w_{01}(y) + (\epsilon \cos \omega t) w_{11}(y), \quad (3.1)$$

$$u_2(y,t) = u_{02}(y) + (\epsilon \cos \omega t) u_{12}(y) \quad \text{and} \quad w_2(y,t) = w_{02}(y) + (\epsilon \cos \omega t) w_{12}(y), \quad (3.2)$$

$$\theta_1(y,t) = \theta_{01}(y) + (\epsilon \cos \omega t) \theta_{11}(y) \quad \text{and} \quad \theta_2(y,t) = \theta_{02}(y) + (\epsilon \cos \omega t) \theta_{12}(y) \quad (3.3)$$

where, for steady state $u_{01}, u_{02}, w_{01}, w_{02}$ and θ_{01}, θ_{02} are the velocity and temperature components; while $u_{11}, u_{12}, w_{11}, w_{12}$, and θ_{11}, θ_{12} are the associated time dependent parts in the two fluid zones. The following differential equations are produced individually by putting the Eqs (3.1-3.3) into the Eqs (2.2, 2.3, 2.4, 2.7, 2.8, and 2.9) and then separating the steady and transient time varying components. With the help of conditions (2.12-2.16), the resulting equations are solved analytically. The closed form solutions for both steady and transient time varied parts are obtained separately to obtain solutions to the issue of an unsteady motion in two liquid zones.

Region-I

$$\frac{d^2 q_{01}}{dy^2} - b_2 q_{01} = b_3, \quad (3.4)$$

$$\frac{d^2 q_{11}}{dy^2} - (b_2 - \omega \tan \omega t) q_{11} = 0, \quad (3.5)$$

$$\frac{1}{P_{r1}} \frac{d^2 \theta_{01}}{dy^2} = - \left(\frac{dq_{01}}{dy} \frac{d\bar{q}_{01}}{dy} \right) - \left(q_{01} a_9 \bar{q}_{01} a_9 + q_{01} a_9 \bar{a}_{10} + \bar{q}_{01} a_9 a_{10} + a_{10} \bar{a}_{10} \right) M^2, \quad (3.6)$$

$$\frac{1}{Pr_1} \frac{d^2 \theta_{11}}{dy^2} + \omega \tan \omega t \theta_{11} = - \left(\frac{dq_{11}}{dy} \frac{d\bar{q}_{01}}{dy} - \frac{dq_{01}}{dy} \frac{d\bar{q}_{11}}{dy} \right) - \epsilon \cos \omega t \left(\frac{dq_{11}}{dy} \frac{d\bar{q}_{11}}{dy} \right) + \quad (3.7)$$

$$- \left(\overline{q_{01} q_{11} a_9 a_9} + \overline{a_9 a_9 q_{01} q_{11}} + \epsilon \cos \omega t \overline{a_9 a_9 q_{11} q_{11}} + \overline{q_{11} a_9 a_{10}} + \overline{a_{10} a_9 q_{11}} \right) M^2.$$

Region-II

$$\frac{d^2 q_{02}}{dy^2} - b_5 q_{02} = b_6, \quad (3.8)$$

$$\frac{d^2 q_{12}}{dy^2} - (b_5 - \omega \tan \omega t) q_{12} = 0, \quad (3.9)$$

$$\frac{1}{Pr_2} \frac{d^2 \theta_{02}}{dy^2} = - \left(\frac{dq_{02}}{dy} \frac{d\bar{q}_{02}}{dy} \right) \frac{\beta}{\alpha} + \quad (3.10)$$

$$- \left(\overline{a_{14} a_{14} q_{02} q_{02}} + \overline{a_{15} a_{14} q_{02}} + \overline{a_{15} a_{14} q_{02}} + \overline{a_{15} a_{15}} \right) h^2 M^2 \sigma \beta,$$

$$\frac{1}{Pr_2} \frac{d^2 \theta_{12}}{dy^2} + \omega \tan \omega t \theta_{12} = - \left\{ \left(\frac{dq_{02}}{dy} \frac{d\bar{q}_{12}}{dy} + \frac{dq_{12}}{dy} \frac{d\bar{q}_{02}}{dy} \right) + \epsilon \cos \omega t \left(\frac{dq_{12}}{dy} \frac{d\bar{q}_{12}}{dy} \right) \right\} \frac{\beta}{\alpha} + \quad (3.11)$$

$$- \left\{ \overline{a_{14} a_{14} q_{02} q_{12}} + \overline{a_{14} a_{14} q_{12} q_{02}} + \epsilon \cos \omega t \left(\overline{a_{14} a_{14} q_{12} q_{12}} \right) + \right.$$

$$\left. + \overline{a_{15} a_{14} q_{12}} + \overline{a_{14} a_{15} q_{12}} \right\} h^2 M^2 \sigma \beta.$$

Related conditions are given by

Steady state:

$$\text{at } y = l, q_{01} = 0 \text{ and } q_{02} = 0 \text{ at } y = -l, \quad (3.12)$$

$$\text{At the interface } y = 0: q_{01}(0) = q_{02}(0), \frac{dq_{01}}{dy} = \frac{1}{\alpha h} \frac{dq_{02}}{dy}, \quad (3.13)$$

$$\theta_{01}(l) = 0, \theta_{02}(-l) = 0, \quad (3.14)$$

$$\text{at } y = 0: \theta_{01}(0) = \theta_{02}(0) \text{ and } \frac{d\theta_{01}}{dy} = \frac{1}{\beta h} \frac{d\theta_{02}}{dy}. \quad (3.15)$$

Transient time dependent part

$$q_{11}(l) = 0 \text{ and } q_{12}(-l) = 0. \quad (3.16)$$

$$q_{11}(0)=q_{12}(0) \text{ and } \frac{dq_{11}}{dy} = \frac{1}{\alpha h} \frac{dq_{12}}{dy} \text{ at } y=0, \tag{3.17}$$

$$\theta_{11}(l)=0, \theta_{12}(-l)=0, \tag{3.18}$$

$$\theta_{11}(0)=\theta_{12}(0) \text{ and } \frac{d\theta_{11}}{dy} = \frac{1}{\beta h} \frac{d\theta_{12}}{dy} \text{ at the interface } y=0. \tag{3.19}$$

By solving the above set of equations from (3.4)-(3.11) with the help of conditions (3.12)-(3.19), the following expressions are acquired for the velocity, temperature and rates of heat transfer coefficients as:

Region-I:

$$q_1(y,t) = q_{01}(y) + \epsilon \cos \omega t q_{11}(y) = B_1 e^{b_{14}y} + B_2 e^{b_{15}y} - b_{16} + \epsilon \cos \omega t (B_5 e^{b_{20}y} + B_6 e^{b_{21}y}), \tag{3.20}$$

$$\begin{aligned} \theta_1(y,t) = \theta_{01}(y) + (\epsilon \cos \omega t) \theta_{11}(y) = & B_9 + B_{10}y + b_{30}e^{(b_{14}+\bar{b}_{14})y} + b_{31}e^{(b_{14}+\bar{b}_{15})y} + \\ & + b_{32}e^{(b_{15}+\bar{b}_{14})y} + b_{33}e^{(b_{15}+\bar{b}_{15})y} + b_{34}e^{b_{14}y} + b_{35}e^{b_{15}y} + b_{36}e^{\bar{b}_{14}y} + b_{37}e^{\bar{b}_{15}y} + b_{38}y^2 + \\ & + \epsilon \cos \omega t [B_{13}e^{b_{39}y} + B_{14}e^{b_{40}y} + b_{41}e^{(b_{20}+\bar{b}_{20})y} + b_{42}e^{(b_{20}+\bar{b}_{21})y} + b_{43}e^{(b_{21}+\bar{b}_{20})y} + \\ & + b_{44}e^{(b_{21}+\bar{b}_{21})y} + b_{45}e^{(b_{14}+\bar{b}_{20})y} + b_{46}e^{(b_{14}+\bar{b}_{21})y} + b_{47}e^{(b_{15}+\bar{b}_{20})y} + b_{48}e^{(b_{15}+\bar{b}_{21})y} + \\ & + b_{49}e^{(b_{20}+\bar{b}_{14})y} + b_{50}e^{(b_{20}+\bar{b}_{15})y} + b_{51}e^{(b_{21}+\bar{b}_{14})y} + b_{52}e^{(b_{21}+\bar{b}_{15})y} + b_{53}e^{\bar{b}_{20}y} + \\ & + b_{54}e^{\bar{b}_{21}y} + b_{55}e^{b_{20}y} + b_{56}e^{b_{21}y}], \end{aligned} \tag{3.21}$$

$$\begin{aligned} Nu_l = - \left(\frac{\partial \theta_1}{\partial y} \right)_{\text{at } y=l} = & - \left\{ 2b_{38} + B_{10} + b_{30}(b_{14} + \bar{b}_{14})e^{(b_{14}+\bar{b}_{14})} + \right. \\ & + b_{31}(b_{14} + \bar{b}_{15})e^{(b_{14}+\bar{b}_{15})} + b_{32}(b_{15} + \bar{b}_{14})e^{(b_{15}+\bar{b}_{14})} + b_{33}(b_{15} + \bar{b}_{15})e^{(b_{15}+\bar{b}_{15})} + \\ & + b_{34}b_{14}e^{b_{14}} + b_{35}b_{15}e^{b_{15}} + b_{36}\bar{b}_{14}e^{\bar{b}_{14}} + b_{37}\bar{b}_{15}e^{\bar{b}_{15}} + \epsilon \cos \omega t [B_{13}b_{39}e^{b_{39}} + \\ & + B_{14}b_{40}e^{b_{40}} + b_{41}(b_{20} + \bar{b}_{20})e^{(b_{20}+\bar{b}_{20})} + b_{42}(b_{20} + \bar{b}_{21})e^{(b_{20}+\bar{b}_{21})} + \\ & + b_{43}(b_{21} + \bar{b}_{20})e^{(b_{21}+\bar{b}_{20})} + b_{44}(b_{21} + \bar{b}_{21})e^{(b_{21}+\bar{b}_{21})} + b_{45}(b_{14} + \bar{b}_{20})e^{(b_{14}+\bar{b}_{20})} + \\ & + b_{46}(b_{14} + \bar{b}_{21})e^{(b_{14}+\bar{b}_{21})} + b_{47}(b_{15} + \bar{b}_{20})e^{(b_{15}+\bar{b}_{20})} + b_{48}(b_{15} + \bar{b}_{21})e^{(b_{15}+\bar{b}_{21})} + \\ & + b_{49}(b_{20} + \bar{b}_{14})e^{(b_{20}+\bar{b}_{14})} + b_{50}(b_{20} + \bar{b}_{15})e^{(b_{20}+\bar{b}_{15})} + b_{51}(b_{21} + \bar{b}_{14})e^{(b_{21}+\bar{b}_{14})} + \\ & \left. + b_{52}(b_{21} + \bar{b}_{15})e^{(b_{21}+\bar{b}_{15})} + b_{53}\bar{b}_{20}e^{\bar{b}_{20}} + b_{54}\bar{b}_{21}e^{\bar{b}_{21}} + b_{55}b_{20}e^{b_{20}} + b_{56}b_{21}e^{b_{21}} \right\}. \end{aligned} \tag{3.22}$$

Region-II:

$$q_2(y,t) = q_{02}(y) + \epsilon \cos \omega t q_{12}(y) = B_3 e^{b_{17}y} + B_4 e^{b_{18}y} - b_{19} + \epsilon \cos \omega t (B_7 e^{b_{22}y} + B_8 e^{b_{23}y}), \tag{3.23}$$

$$\begin{aligned}
\theta_2(y,t) = \theta_{02}(y) + (\varepsilon \cos \omega t) \theta_{12}(y) = & B_{11} + B_{12}y + b_{57}e^{(b_{17}+\bar{b}_{17})y} + b_{58}e^{(b_{17}+\bar{b}_{18})y} + \\
& + b_{59}e^{(b_{18}+\bar{b}_{17})y} + b_{60}e^{(b_{18}+\bar{b}_{18})y} + b_{61}e^{\bar{b}_{17}y} + b_{62}e^{\bar{b}_{18}y} + b_{63}e^{b_{17}y} + b_{64}e^{b_{18}y} + b_{65}y^2 + \\
& + \varepsilon \cos \omega t \left[B_{15}e^{b_{66}y} + B_{16}e^{b_{67}y} + b_{66}e^{(b_{22}+\bar{b}_{22})y} + b_{67}e^{(b_{22}+\bar{b}_{23})y} + b_{68}e^{(b_{23}+\bar{b}_{22})y} + \right. \\
& + b_{69}e^{(b_{23}+\bar{b}_{23})y} + b_{70}e^{(b_{22}+\bar{b}_{17})y} + b_{71}e^{(b_{22}+\bar{b}_{18})y} + b_{72}e^{(b_{23}+\bar{b}_{18})y} + b_{73}e^{(b_{23}+\bar{b}_{17})y} + \\
& + b_{74}e^{(b_{17}+\bar{b}_{22})y} + b_{75}e^{(b_{18}+\bar{b}_{22})y} + b_{76}e^{(b_{17}+\bar{b}_{23})y} + b_{77}e^{(b_{18}+\bar{b}_{23})y} + b_{78}e^{\bar{b}_{22}y} + b_{79}e^{\bar{b}_{23}y} + \\
& \left. b_{80}e^{b_{22}y} + b_{81}e^{b_{23}y} \right], \tag{3.24}
\end{aligned}$$

$$\begin{aligned}
Nu_2 = \frac{I}{\beta h} \left(\frac{\partial \theta_2}{\partial y} \right)_{\text{at } y = -1} = & -\frac{I}{\beta h} \left\{ B_{12} - 2b_{65} + b_{57}(b_{17} + \bar{b}_{17})e^{-(b_{17}+\bar{b}_{17})} + \right. \\
& + b_{58}(b_{17} + \bar{b}_{18})e^{-(b_{17}+\bar{b}_{18})} + b_{59}(b_{18} + \bar{b}_{17})e^{-(b_{18}+\bar{b}_{17})} + b_{60}(b_{18} + \bar{b}_{18})e^{-(b_{18}+\bar{b}_{18})} + \\
& + b_{61}\bar{b}_{17}e^{-\bar{b}_{17}} + b_{62}\bar{b}_{18}e^{-\bar{b}_{18}} + b_{63}b_{17}e^{-b_{17}} + b_{64}b_{18}e^{-b_{18}} + \varepsilon \cos \omega t \left[B_{15}b_{66}e^{-b_{66}} + \right. \\
& + B_{16}b_{67}e^{-b_{67}} + b_{66}(b_{22} + \bar{b}_{22})e^{-(b_{22}+\bar{b}_{22})} + b_{67}(b_{22} + \bar{b}_{23})e^{-(b_{22}+\bar{b}_{23})} + \\
& + b_{68}(b_{23} + \bar{b}_{22})e^{-(b_{23}+\bar{b}_{22})} + b_{69}(b_{23} + \bar{b}_{23})e^{-(b_{23}+\bar{b}_{23})} + b_{70}(b_{22} + \bar{b}_{17})e^{-(b_{22}+\bar{b}_{17})} + \\
& + b_{71}(b_{22} + \bar{b}_{18})e^{-(b_{22}+\bar{b}_{18})} + b_{72}(b_{23} + \bar{b}_{18})e^{-(b_{23}+\bar{b}_{18})} + b_{73}(b_{23} + \bar{b}_{17})e^{-(b_{23}+\bar{b}_{17})} + \\
& + b_{74}(b_{17} + \bar{b}_{22})e^{-(b_{17}+\bar{b}_{22})} + b_{75}(b_{18} + \bar{b}_{22})e^{-(b_{18}+\bar{b}_{22})} + b_{76}(b_{17} + \bar{b}_{23})e^{-(b_{17}+\bar{b}_{23})} + \\
& \left. + b_{77}(b_{18} + \bar{b}_{23})e^{-(b_{18}+\bar{b}_{23})} + b_{78}\bar{b}_{22}e^{-\bar{b}_{22}} + b_{79}\bar{b}_{23}e^{-\bar{b}_{23}} + b_{80}b_{22}e^{-b_{22}} + b_{81}b_{23}e^{-b_{23}} \right] \left. \right\} \tag{3.25}
\end{aligned}$$

where, some of the notations/symbols which are involved in the above solutions are represented by:

$$q_1 = q_{01} + (\varepsilon \cos \omega t) q_{11}, \quad q_2 = q_{02} + (\varepsilon \cos \omega t) q_{12},$$

$$\theta_1 = \theta_{01} + (\varepsilon \cos \omega t) \theta_{11}, \quad \theta_2 = \theta_{02} + (\varepsilon \cos \omega t) \theta_{12},$$

$$q_1(y,t) = u_1(y,t) + iw_1(y,t), \quad q_2(y,t) = u_2(y,t) + iw_2(y,t),$$

$$b_1 = P_1 + iP_2, \quad b_2 = \left(\frac{1 - mi}{1 + m^2} \right) M^2 - 2iK^2,$$

$$P_1 = 1 - \frac{m^2 s}{1 + m^2}, \quad P_2 = \frac{-ms}{1 + m^2}, \quad P_3 = 1 - \left(1 - \frac{\sigma_0 \sigma_1}{1 + m^2} \right) s,$$

$$P_4 = \frac{-\sigma_0 \sigma_2 ms}{1 + m^2}, \quad b_3 = -b_1, \quad b_4 = P_3 + iP_4,$$

$$b_5 = (\sigma_1 - i\sigma_2 m) \frac{\alpha h^2 M^2}{1+m^2} - 2ih^2 K^2 \rho \alpha, \quad b_6 = -b_4 \alpha h^2,$$

$$b_7 = \frac{1-mi}{(1+m^2)}, \quad b_8 = \frac{s}{M^2} \left(i + \frac{m(1-i)}{1+m^2} \right),$$

$$b_9 = -b_8, \quad b_{10} = \frac{i\sigma_0\sigma_1 + m\sigma_0\sigma_2}{1+m^2}, \quad b_{11} = \frac{\sigma_0\sigma_1 - m\sigma_0\sigma_2 i}{1+m^2},$$

$$b_{12} = \frac{(s\sigma_0^2\sigma_2)m}{(1+m^2)M^2} - \left(1 - \frac{\sigma_0\sigma_1}{1+m^2} \right) \frac{is\sigma_0}{M^2} \quad \text{etc.}$$

and the expressions for the remaining coefficients are not provided as they are too many.

4. Results and discussion

For the case of conducting plates, the main equations of motion, current, and energy of an unsteady issue are described. The main and transverse velocity fields: u_1, u_2 and w_1, w_2 as well as the temperature fields θ_1 and θ_2 in the two liquids are solved using the associated equations. The computational estimates for various sets of flow parameter values are resolved to and depicted in Figs.1 to 42. Solid lines represent unsteady flow patterns, while dash-spot lines represent steady flow motions. The effect of control parameters such as the Hartmann number M , Hall parameter m , rotation parameter K , viscosity ratio α , height ratio h , also σ_0 and β as the proportion of electrical and thermal conductivities on the flow and temperature fields is discussed for two situations, namely: $s=0$ and s equal to half of its estimate. In the numerical calculations, we used $\sigma_{01} = 1.2$, $\sigma_{02} = 1.5$, $P_{r1} = 1 = P_{r2}$. In contrast to non-conducting (insulating) plates, (c.f. study of L.Raju and Venkat [43]), the solutions of the present study are observed to rely on s (electron pressure to total pressure ratio) if the plates are conducting in nature. The theoretical results of this study coincide with those of Raju [31] for a steady flow without the rotation component.

In the case of electron-to-total pressure ratio $s = 0$:

Figures 1-3, show the effect of changing the Hartman number M on velocity and temperature. Figures 1 and 2 show that when M increases, both the primary and secondary velocity distributions decrease. This is due to the Lorentz force, which opposes the flow and causes a decrease in velocity. The maximum primary and secondary velocity distributions of the channel begin to migrate below the channel centre line, towards region-II, as M increases. Figure 3 shows that as the value of M rises, the temperature distribution in both zones diminishes. The maximum temperature in the channel tends to shift above the channel centre line towards region-1 as M augments while all of the remaining regulating parameters are fixed.

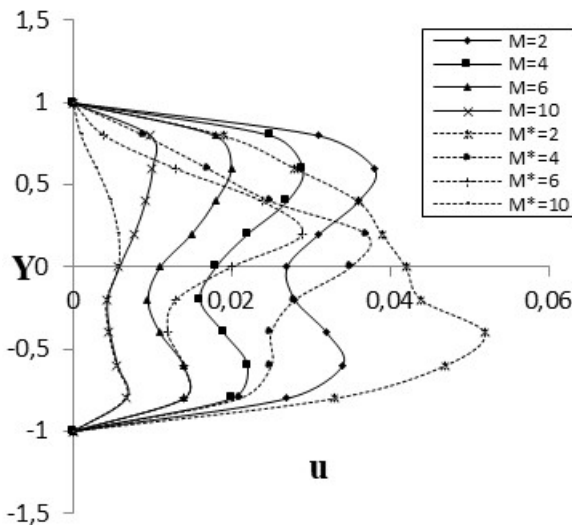


Fig.1. Primary velocity profiles u_1, u_2 (unsteady flow), u_1^*, u_2^* (steady flow) for various M and $m=2$, $\alpha=0.9$, $h=1$, $\sigma_0=1$, $K=2$, $\sigma_1=1.2$, $\sigma_2=1.5$, $\varepsilon=0.5$, $\rho=1$, $\omega=1$, $t=\pi/\omega$, $s=0$ (Conducting plates)

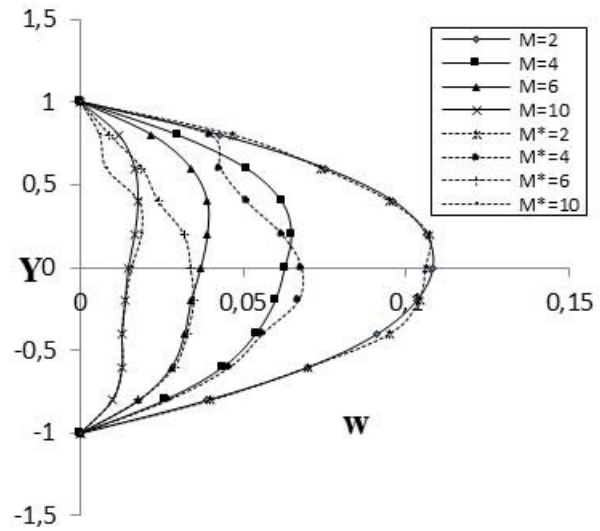


Fig.2. Secondary velocity profiles w_1, w_2 (unsteady flow), w_1^*, w_2^* (steady flow) for various M and $m=2$, $\alpha=0.9$, $h=1$, $K=2$, $\sigma_0=1$, $\sigma_1=1.2$, $\sigma_2=1.5$, $\varepsilon=0.5$, $\rho=1$, $\omega=1$, $t=\pi/\omega$, $s=0$ (Conducting plates)

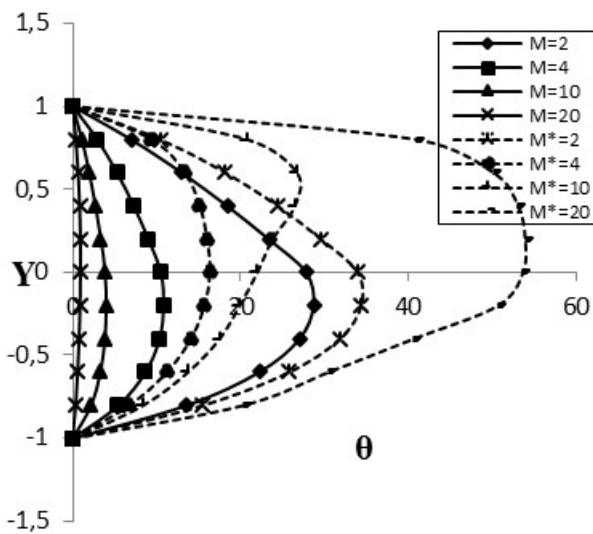


Fig.3. Temperature profiles θ_1, θ_2 (unsteady flow), θ_1^*, θ_2^* (steady flow) for various M and $m=2$, $\alpha=0.333$, $h=0.75$, $\sigma_0=2$, $\sigma_1=1.2$, $\sigma_2=1.5$, $K=1$, $\beta=1$, $\varepsilon=0.5$, $\rho=1$, $\omega=1$, $t=\pi/\omega$, $s=0$ (Conducting plates)

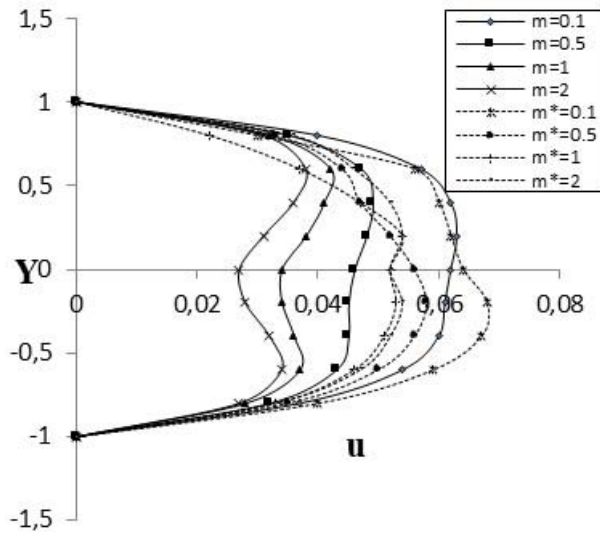


Fig.4. Primary velocity profiles u_1, u_2 (unsteady flow), u_1^*, u_2^* (steady flow) for various m and $M=2$, $\alpha=0.9$, $h=1$, $K=2$, $\sigma_0=1$, $\sigma_1=1.2$, $\sigma_2=1.5$, $\varepsilon=0.5$, $\rho=1$, $\omega=1$, $t=\pi/\omega$, $s=0$ (Conducting plates)

The effect of increasing the Hall parameter m on velocity and temperature fields in the two sites is shown in Figs 4-6. As m increases, the primary velocity distribution in both regions decreases, while the secondary velocity distribution in both regions increases, as seen in Figs 4-5. This could be due to the existence of magnetic damping and Coriolis forces in the flow field, with the Coriolis force causing the so-

called secondary velocity. The maximum primary and secondary velocity distributions of the channel tend to migrate below the channel centre line, towards region-II, as m increases. Figure 6 shows that as the value of m grows, the temperature distribution in both zones decreases. The maximum temperature distribution in the channel tends to shift above the channel centre line, towards region-I, as the Hall parameter m increases.

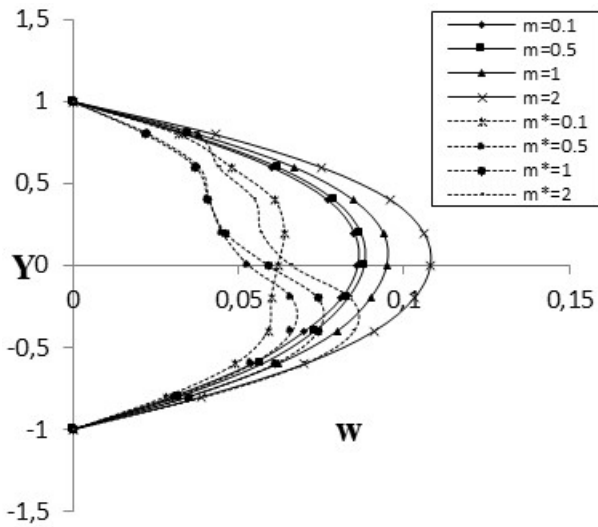


Fig.5. Secondary velocity profiles w_1, w_2 (unsteady flow), w_1^*, w_2^* (steady flow) for various m and $M = 2, \alpha = 0.9, h = 1, K = 2, \sigma_0 = 1, \sigma_1 = 1.2, \sigma_2 = 1.5, \varepsilon = 0.5, \rho = 1, \omega = 1, t = \pi / \omega, s = 0$ (Conducting plates)

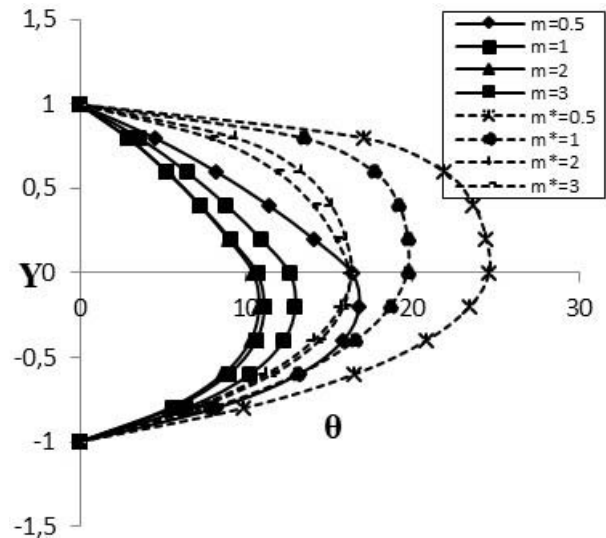


Fig.6. Temperature profiles θ_1, θ_2 (unsteady flow), θ_1^*, θ_2^* (steady flow) for various m and $M = 4, \alpha = 0.333, h = 0.75, \sigma_0 = 2, \sigma_1 = 1.2, \sigma_2 = 1.5, K = 1, \beta = 1, \varepsilon = 0.5, \rho = 1, \omega = 1, t = \pi / \omega, s = 0$ (Conducting plates)

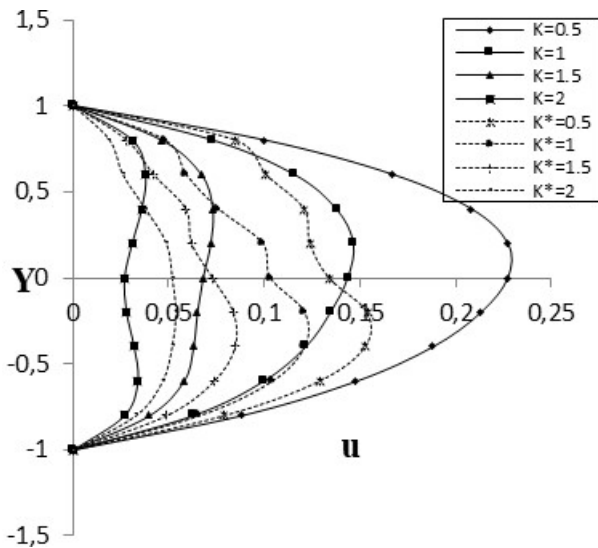


Fig.7. Primary velocity profiles u_1, u_2 (unsteady flow), u_1^*, u_2^* (steady flow) for various K and $M = 2, m = 2, \alpha = 0.9, h = 1, \sigma_0 = 1, \sigma_1 = 1.2, \sigma_2 = 1.5, \varepsilon = 0.5, \rho = 1, \omega = 1, t = \pi / \omega, s = 0$ (Conducting plates)

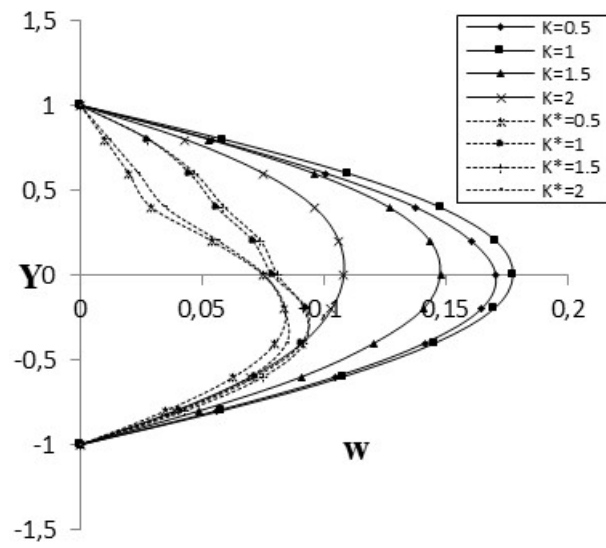


Fig.8. Secondary velocity profiles w_1, w_2 (unsteady flow), w_1^*, w_2^* (steady flow) for various K and $M = 2, m = 2, \alpha = 0.9, h = 1, \sigma_0 = 1, \sigma_1 = 1.2, \sigma_2 = 1.5, \varepsilon = 0.5, \rho = 1, \omega = 1, t = \pi / \omega, s = 0$ (Conducting plates)

Figures 7-9 depict the effect of the Taylor number K on the main and secondary velocity as well as temperature distributions. Increases in K reduce primary velocity distribution in both zones, as shown in Fig.7. The secondary velocity distribution in both zones grows up to $K = 1$ and then declines, as seen in Fig.8. This may be due to the presence of Coriolis forces in the rotating framework and magnetic field. The highest secondary velocity dispersion of the channel began to drift above the channel centre line, towards region-I, as K increased. Figure 9 depicts the effect of the Taylor number K on the temperature distribution in two liquid zones. As the value of K rises, the temperature dispersion between the two zones decreases. The maximum temperature in the channel tends to shift below the channel centre line toward region-II as the Taylor number K grows.

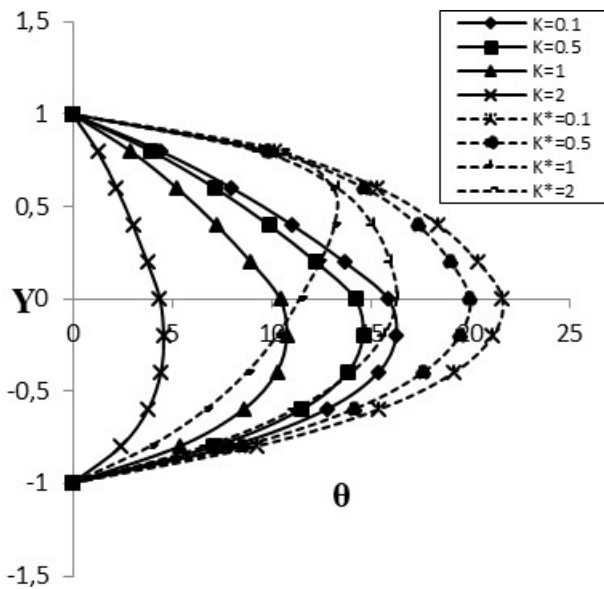


Fig.9. Temperature profiles θ_1, θ_2 (unsteady flow), θ_1^*, θ_2^* (steady flow) for various K and $M = 4$, $m = 2$, $\alpha = 0.333$, $h = 0.75$, $\sigma_0 = 2$, $\sigma_1 = 1.2$, $\sigma_2 = 1.5$, $\beta = 1$, $\varepsilon = 0.5$, $\rho = 1$, $\omega = 1$, $t = \pi / \omega$, $s = 0$ (Conducting plates)

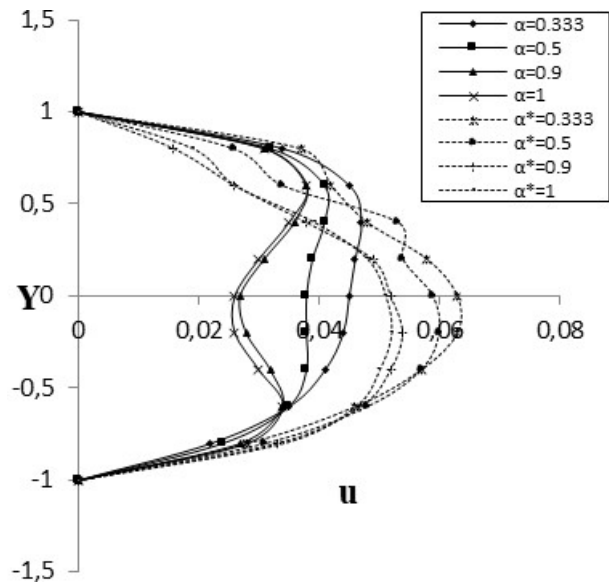


Fig.10. Primary velocity profiles u_1, u_2 (unsteady flow), u_1^*, u_2^* (steady flow) for various α and $M = 2$, $m = 2$, $h = 1$, $K = 2$, $\sigma_0 = 1$, $\sigma_1 = 1.2$, $\sigma_2 = 1.5$, $\varepsilon = 0.5$, $\rho = 1$, $\omega = 1$, $t = \pi / \omega$, $s = 0$ (Conducting plates)

The influence of the viscosity ratio α on the primary and secondary velocity distributions of the two fluids is shown in Figs 10-11. As seen in Figs 10 and 11, the primary velocity distribution in the two regions decreases as α grows, whereas the secondary velocity distribution increases. The maximum primary and secondary velocity distributions of the channel begin to shift above the channel center-line, towards region-I, as α increases. The influence of the viscosity ratio on temperature is depicted in Fig.12, which shows that increasing α decreases the temperature distribution until it reaches $\alpha = 0.5$, at which point it grows in both zones. The temperature distribution in the channel continues to shift below the channel centre line, towards region-II, as α rises.

The influence of the height ratio h on the primary, secondary velocity and temperature distributions is shown in Figs 13-15. As h grows, the primary velocity distribution in region-I diminishes, as illustrated in Fig.13. It rises in region-II until it reaches $h = 1$ and then falls. As seen in Fig.14, the secondary velocity distribution increases with increasing h up to the value of $h = 1$ and then decreases in the region-I. In region-II, increases in h enhance the secondary velocity distribution. The maximum primary and secondary velocity distributions of the channel begin to migrate below the channel centre line, towards region-II, as h increases. Figure 15 shows that increasing h causes the temperature distribution to drop until it reaches $h = 0.5$, at

which point it grows in region-I while decreases in region-II. The maximum temperature in the channel tends to migrate below the channel central axis as h grows, towards region-II.

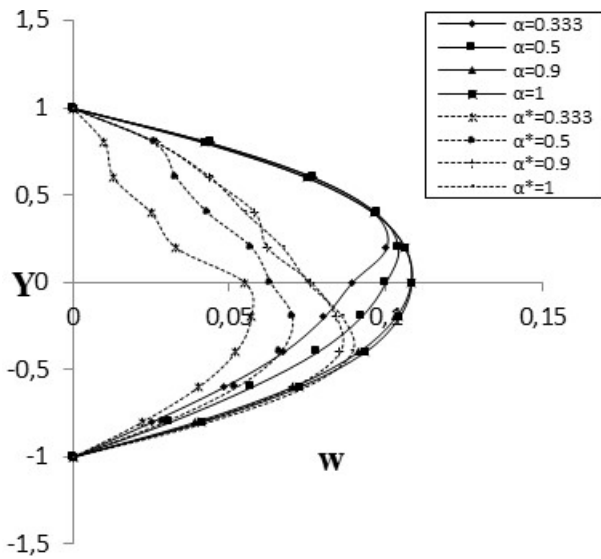


Fig.11. Secondary velocity profiles w_1, w_2 (unsteady flow), w_1^*, w_2^* (steady flow) for various α and $M = 2, m = 2, h = 1, K = 2, \sigma_0 = 1, \sigma_1 = 1.2, \sigma_2 = 1.5, \varepsilon = 0.5, \rho = 1, \omega = 1, t = \pi / \omega, s = 0$ (Conducting plates)

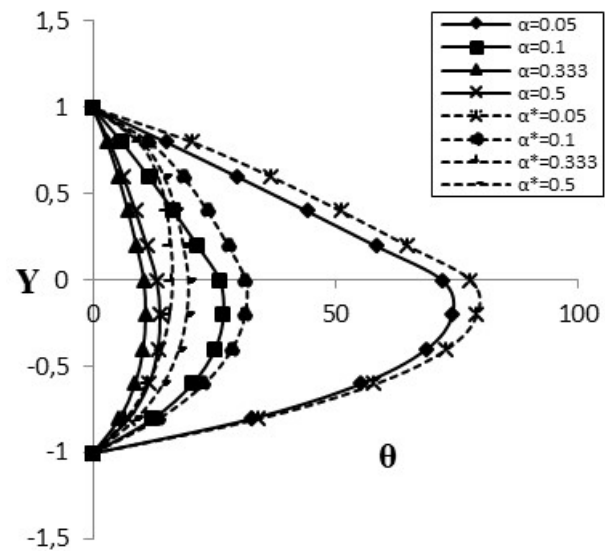


Fig.12. Temperature profiles θ_1, θ_2 (unsteady flow), θ_1^*, θ_2^* (steady flow) for various α and $M = 4, m = 2, h = 0.75, \sigma_0 = 2, \sigma_1 = 1.2, \sigma_2 = 1.5, K = 1, \beta = 1, \varepsilon = 0.5, \rho = 1, \omega = 1, t = \pi / \omega, s = 0$ (Conducting plates)

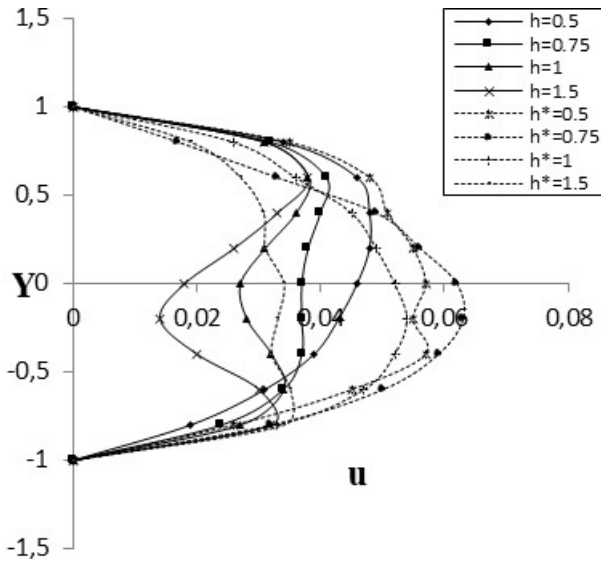


Fig.13. Primary velocity profiles u_1, u_2 (unsteady flow), u_1^*, u_2^* (steady flow) for various h and $M = 2, m = 2, \alpha = 0.9, K = 2, \sigma_0 = 1, \sigma_1 = 1.2, \sigma_2 = 1.5, \varepsilon = 0.5, \rho = 1, \omega = 1, t = \pi / \omega, s = 0$ (Conducting plates)

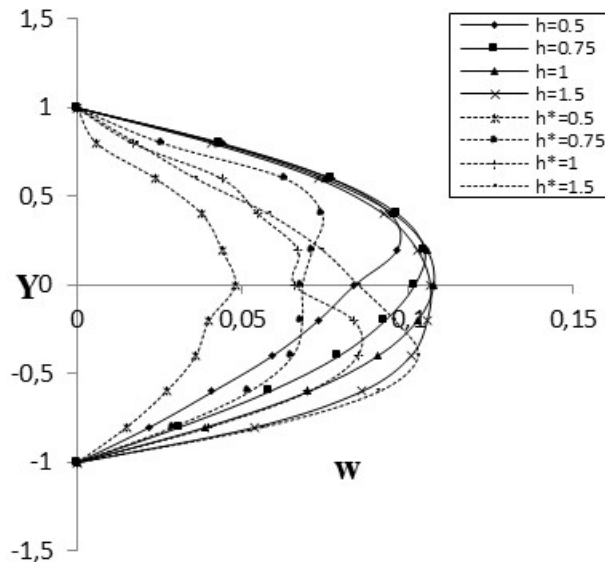


Fig.14. Secondary velocity profiles w_1, w_2 (unsteady flow), w_1^*, w_2^* (steady flow) for various h and $M = 2, m = 2, \alpha = 0.9, K = 2, \sigma_0 = 1, \sigma_1 = 1.2, \sigma_2 = 1.5, \varepsilon = 0.5, \rho = 1, \omega = 1, t = \pi / \omega, s = 0$ (Conducting plates)

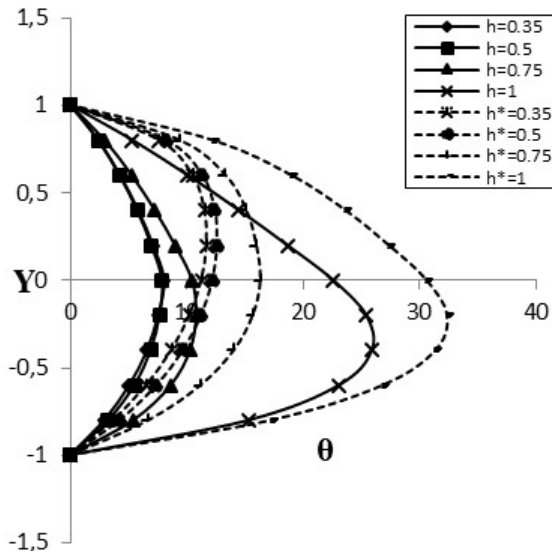


Fig.15. Temperature profiles θ_1, θ_2 (unsteady flow), θ_1^*, θ_2^* (steady flow) for various h and $M = 4, m = 2, \alpha = 0.333, \sigma_0 = 2, \sigma_1 = 1.2, \sigma_2 = 1.5, K = 1, \beta = 1, \varepsilon = 0.5, \rho = 1, \omega = 1, t = \pi / \omega, s = 0$ (Conducting plates)

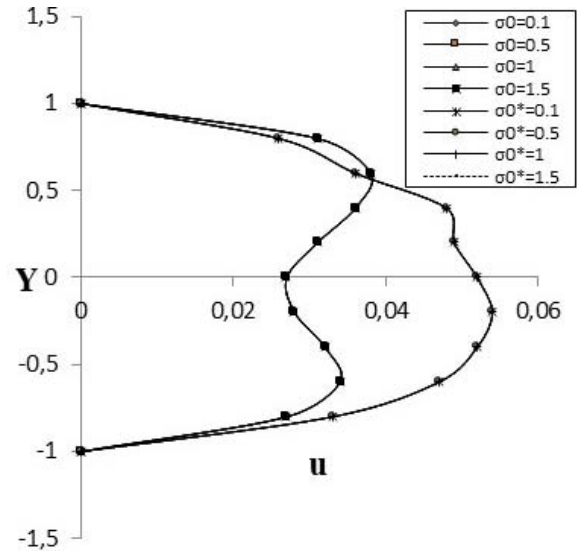


Fig.16. Primary velocity profiles u_1, u_2 (unsteady flow), u_1^*, u_2^* (steady flow) for various σ_0 and $M = 2, m = 2, \alpha = 0.9, h = 1, K = 2, \sigma_1 = 1.2, \sigma_2 = 1.5, \varepsilon = 0.5, \rho = 1, \omega = 1, t = \pi / \omega, s = 0$ (Conducting plates)

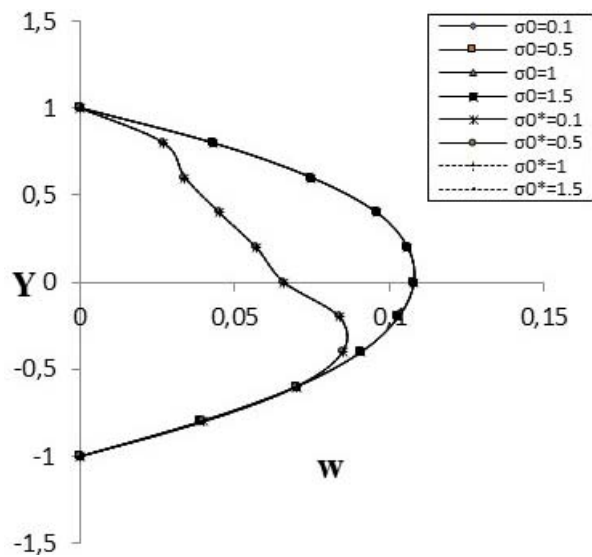


Fig.17. Secondary velocity profiles w_1, w_2 (unsteady flow), w_1^*, w_2^* (steady flow) for various σ_0 and $M = 2, m = 2, \alpha = 0.9, h = 1, K = 2, \sigma_1 = 1.2, \sigma_2 = 1.5, \varepsilon = 0.5, \rho = 1, \omega = 1, t = \pi / \omega, s = 0$ (Conducting plates)

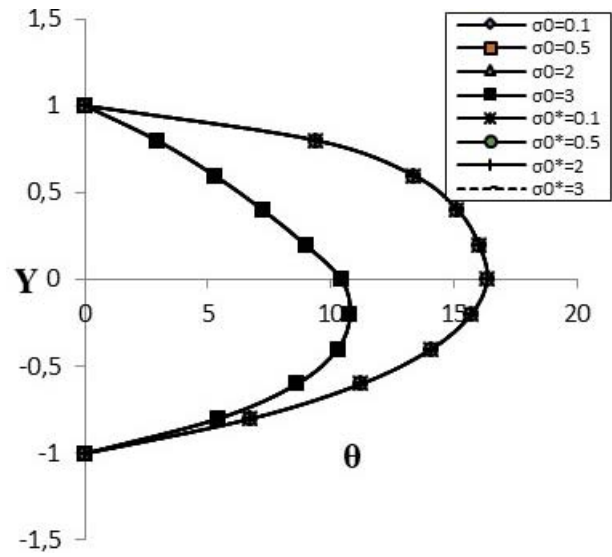


Fig.18. Temperature profiles θ_1, θ_2 (unsteady flow), θ_1^*, θ_2^* (steady flow) for various σ_0 and $M = 2, m = 2, \alpha = 0.333, h = 0.75, \sigma_1 = 1.2, \sigma_2 = 1.5, K = 1, \beta = 1, \varepsilon = 0.5, \rho = 1, \omega = 1, t = \pi / \omega, s = 0$ (Conducting plates)

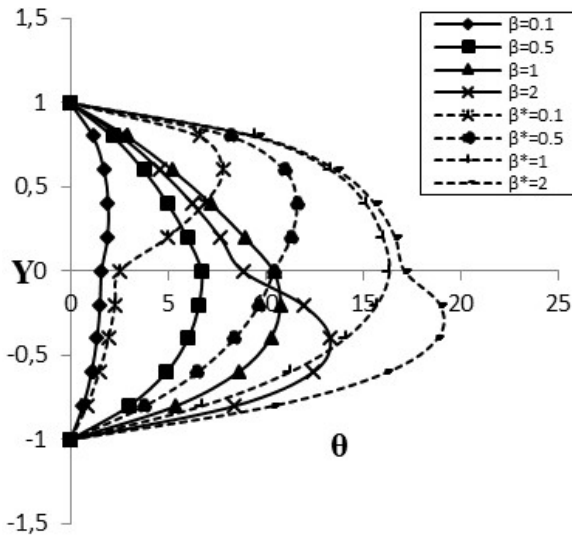


Fig.19. Temperature profiles θ_1, θ_2 (unsteady flow), θ_1^*, θ_2^* (steady flow) for various β and $M = 4, m = 2, \alpha = 0.333, h = 0.75, \sigma_0 = 2, \sigma_1 = 1.2, \sigma_2 = 1.5, K = 1, \epsilon = 0.5, \rho = 1, \omega = 1, t = \pi / \omega, s = 0$ (Conducting plates)

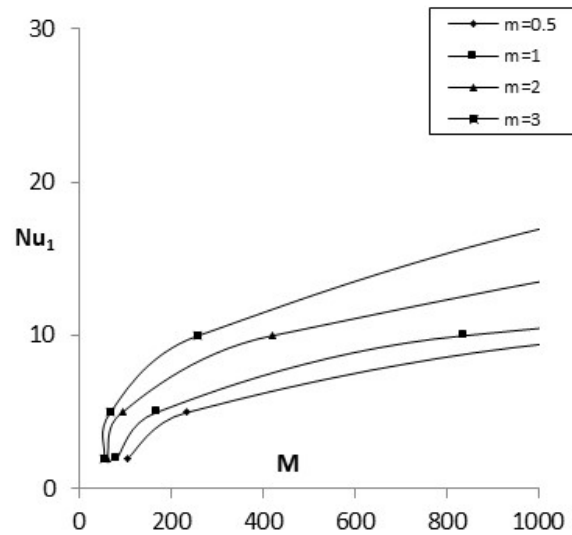


Fig.20. Nusselt Number Nu_1 for various M and $\alpha = 0.333, \sigma_0 = 1, \sigma_1 = 1.2, \sigma_2 = 1.5, h = 0.75, \rho = 1, \beta = 1, K = 1, \epsilon = 0.5, \omega = 1, t = \pi / \omega, s = 0$ (Conducting plates)

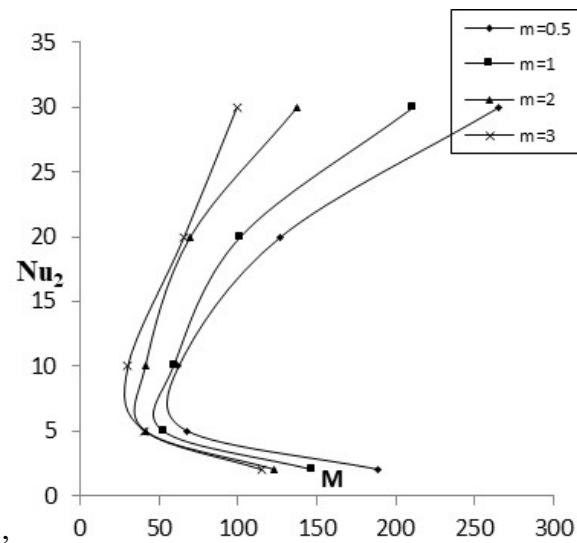


Fig.21. Nusselt Number Nu_2 for various M and $\alpha = 0.333, \sigma_0 = 1, \sigma_1 = 1.2, \sigma_2 = 1.5, h = 0.75, \rho = 1, \beta = 1, K = 1, \epsilon = 0.5, \omega = 1, t = \pi / \omega, s = 0$ (Conducting plates)

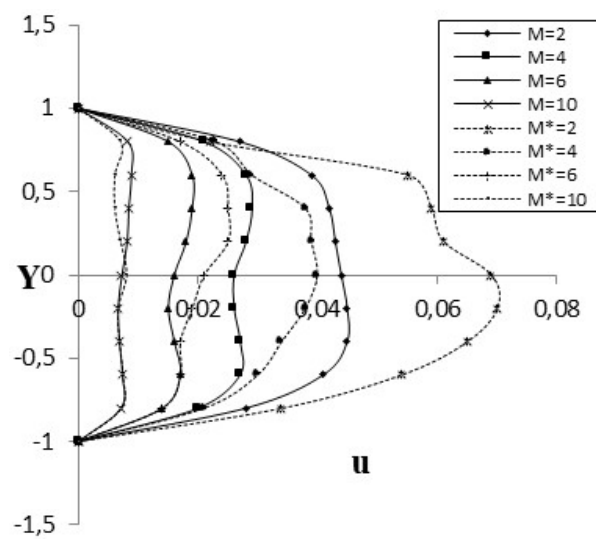


Fig.22. Primary velocity profiles u_1, u_2 (unsteady flow), u_1^*, u_2^* (steady flow) for various M and $m = 2, \alpha = 0.9, h = 1, \sigma_0 = 1, K = 2, \sigma_1 = 1.2, \sigma_2 = 1.5, \epsilon = 0.5, \rho = 1, \omega = 1, t = \pi / \omega, s = 0.5$ (Conducting plates)

Figures 16-18 show how the electrical conductivity ratio σ_0 affects the outcome on velocity and heat distribution. When σ_0 grows, it is revealed that there is no significant variation in the primary and secondary velocity distributions. But maximum primary velocity distribution of the channel tends to move below the

channel centre line towards region-II as σ_0 increases, whereas the maximum secondary velocity distribution tends to move above the channel centre line towards region-I. The temperature distribution in the two zones rises as the parameter σ_0 rises. The maximum velocity distribution of the channel tends to shift above the channel centre line, towards region-I, as σ_0 increases.

Figure 19 depicts the impact of the thermal conductivity ratio β on temperature distribution. It has been shown that when β rises, the temperature distribution rises until it reaches $\beta = 1$, at which time it begins to diminish in region-I while growing in region II. As β increases, the channels maximum temperature tends to drop below the channel centre line, towards region-II. This means that increasing the thermal conductivity ratio β causes the temperature of the fluid to rise faster towards region-II.

Figures 20 and 21 show the rate of heat transfer coefficients versus Hartmann number M for various Hall parameter values. When the remaining parameters are held constant, it is revealed that the rate of heat transfer coefficient increases as M rises. It is also discovered that increasing the hall parameter m up to a specific esteem reduces the rate of heat transfer coefficient at the upper plate and increases past this esteem, while the rate of heat transfer coefficient increases at the lower plate as the hall parameter increases exactly when all the other governing parameters remain constant.

In the case of electron-to-total pressure ratio $s = 1 / 2$:

The effects of the Hartmann number M on the primary and secondary velocity, and temperature distributions of the two fluids are shown in Figs 22-24. The primary and secondary velocity distributions in both zones decrease as M increases. The maximum primary and secondary velocity distributions of the channel begin to migrate above the channel centre line, towards region-I, as M increases. The temperature distribution in both zones grows as M increases up to $M = 4$, then drops as seen in Fig.24. As M grows, the maximum temperature in the channel tends to go above the channel centre line towards region-I when all of the remaining controlling factors are fixed.

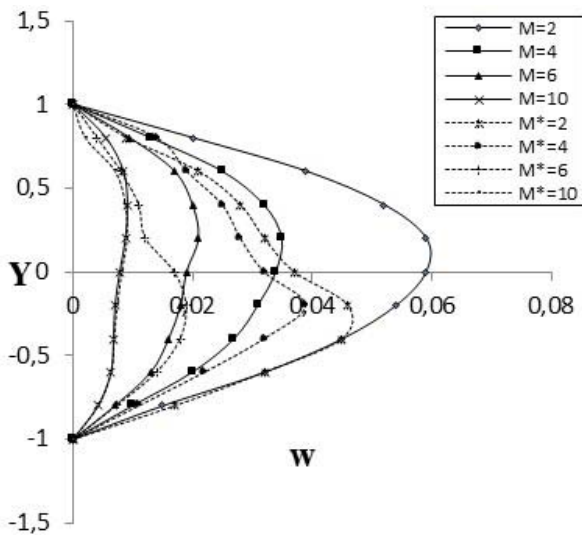


Fig.23. Secondary velocity profiles w_1, w_2 (unsteady flow), w_1^*, w_2^* (steady flow) for various M and $m = 2, \alpha = 0.9, h = 1, K = 2, \sigma_0 = 1, \sigma_1 = 1.2, \sigma_2 = 1.5, \epsilon = 0.5, \rho = 1, \omega = 1, t = \pi / \omega, s = 0.5$ (Conducting plates)

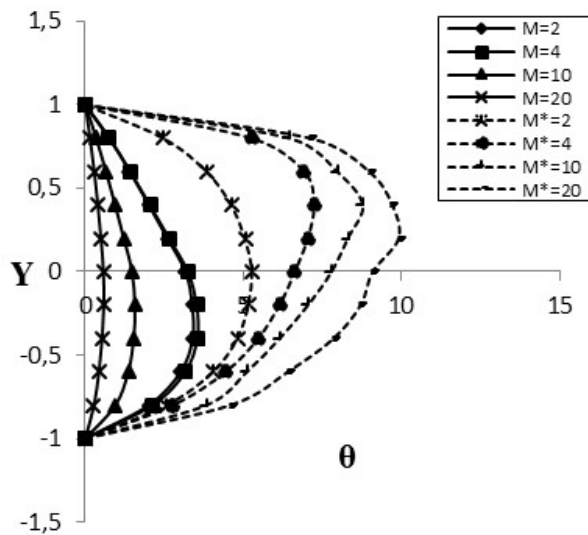


Fig.24. Temperature profiles θ_1, θ_2 (unsteady flow), θ_1^*, θ_2^* (steady flow) for various M and $m = 2, \alpha = 0.333, h = 0.75, \sigma_0 = 2, \sigma_1 = 1.2, \sigma_2 = 1.5, K = 1, \beta = 1, \epsilon = 0.5, \rho = 1, \omega = 1, t = \pi / \omega, s = 0.5$ (Conducting plates)

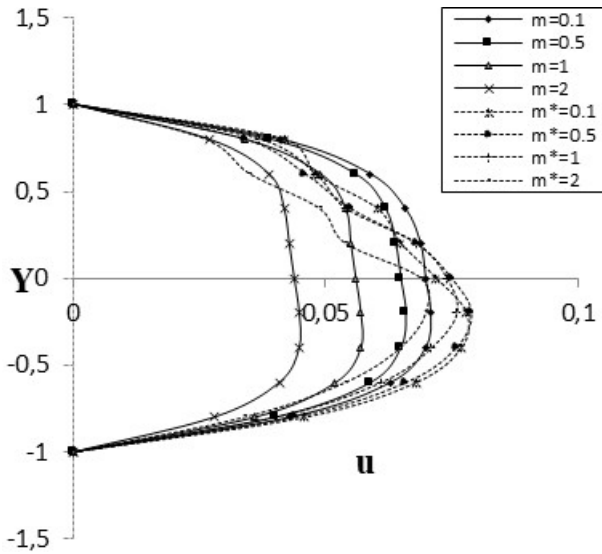


Fig.25. Primary velocity profiles u_1, u_2 (unsteady flow), u_1^*, u_2^* (steady flow) for various m and $M = 2, \alpha = 0.9, h = 1, K = 2, \sigma_0 = 1, \sigma_1 = 1.2, \sigma_2 = 1.5, \epsilon = 0.5, \rho = 1, \omega = 1, t = \pi / \omega, s = 0.5$ (Conducting plates)

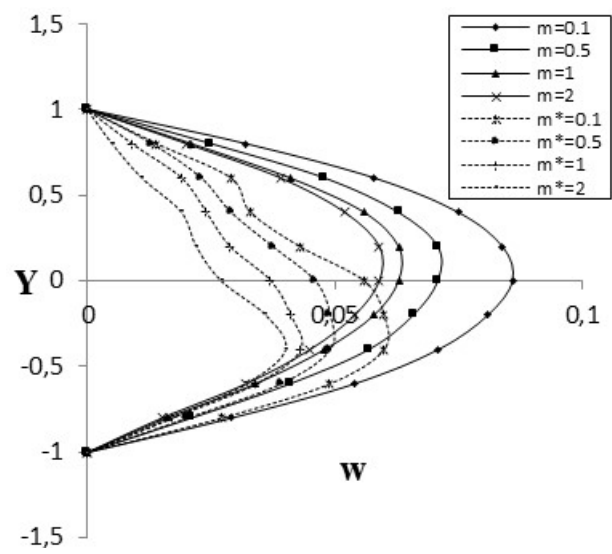


Fig.26. Secondary velocity profiles w_1, w_2 (unsteady flow), w_1^*, w_2^* (steady flow) for various m and $M = 2, \alpha = 0.9, h = 1, K = 2, \sigma_0 = 1, \sigma_1 = 1.2, \sigma_2 = 1.5, \epsilon = 0.5, \rho = 1, \omega = 1, t = \pi / \omega, s = 0.5$ (Conducting plates)

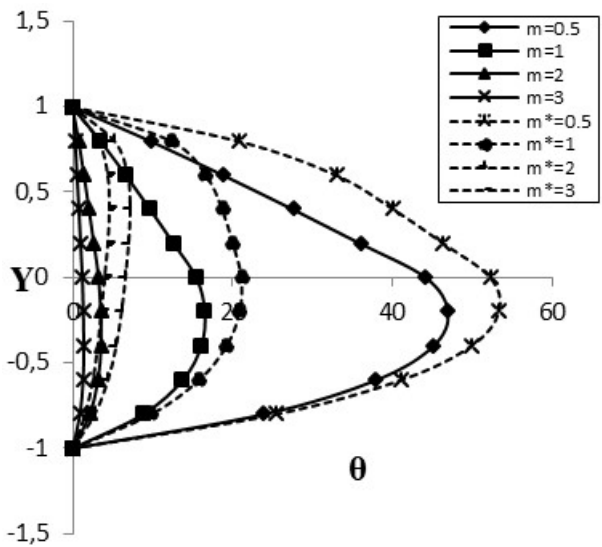


Fig.27. Temperature profiles θ_1, θ_2 (unsteady flow), θ_1^*, θ_2^* (steady flow) for various m and $M = 4, \alpha = 0.333, h = 0.75, K = 1, \beta = 1, \sigma_0 = 2, \sigma_1 = 1.2, \sigma_2 = 1.5, \epsilon = 0.5, \rho = 1, \omega = 1, t = \pi / \omega, s = 0.5$ (Conducting plates)

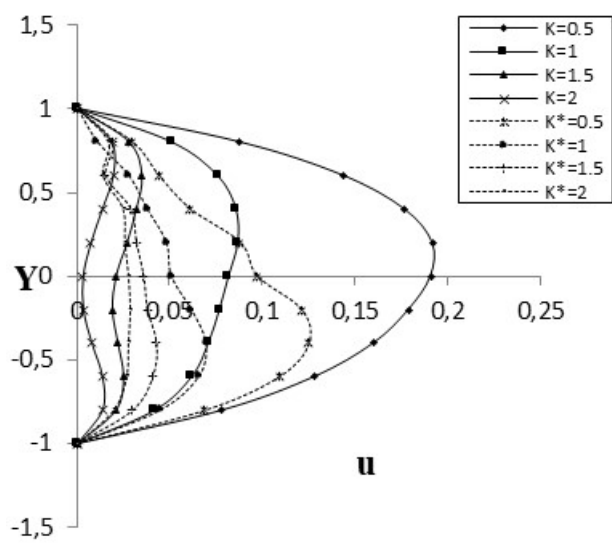


Fig.28. Primary velocity profiles u_1, u_2 (unsteady flow), u_1^*, u_2^* (steady flow) for various K and $M = 2, m = 2, \alpha = 0.9, h = 1, \sigma_0 = 1, \sigma_1 = 1.2, \sigma_2 = 1.5, \epsilon = 0.5, \rho = 1, \omega = 1, t = \pi / \omega, s = 0.5$, (Conducting plates)

The effects of varying the Hall parameter m on velocity and heat distributions in two sites are shown in Figs 25-27. The primary and secondary velocity distributions in the two zones are lower when m

is increased, as illustrated in Figs 23 and 24. The maximum primary and secondary velocity distributions of the channel tend to migrate below the channel centre line, toward region-II, as m increases. As seen in Fig.27 that the temperature distribution in both zones diminishes as the value of m rises. Furthermore, as the Hall parameter m is increased, the maximum temperature distribution in the channel appears to move below the channel centre line towards region-II.

The effect of the Taylor number K on both the main and secondary velocity distributions is shown in Figs 28 and 29. The primary and secondary velocity distributions in the two zones both decrease as K increases. The channels maximum primary and secondary velocity distributions begin to migrate above the channel centre line, towards region-I, as K increases. Figure 30 shows the effect of the Taylor number K on heat flow in two liquid areas. The temperature distribution in the two zones is reduced when K is increased. The maximum temperature within the channel tends to shift above the channel centre line, towards region-I, as the Taylor number K grows.

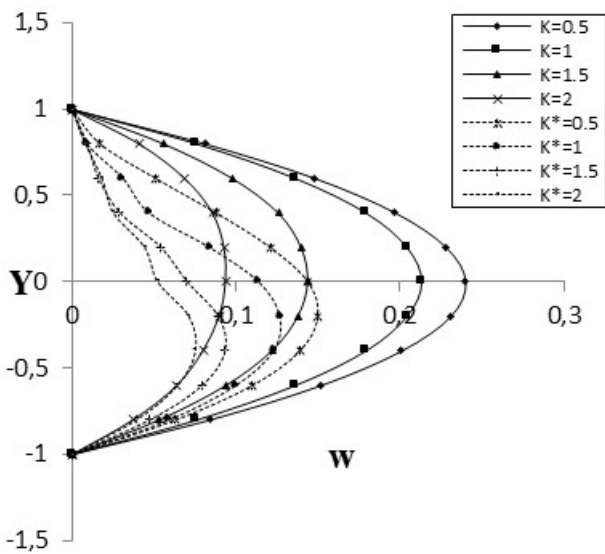


Fig.29. Secondary velocity profiles w_1, w_2 (unsteady flow), w_1^*, w_2^* (steady flow) for various K and $M = 2, m = 2, \alpha = 0.9, h = 1, \sigma_0 = 1, \sigma_1 = 1.2, \sigma_2 = 1.5, \epsilon = 0.5, \rho = 1, \omega = 1, t = \pi / \omega, s = 0.5$ (Conducting plates)

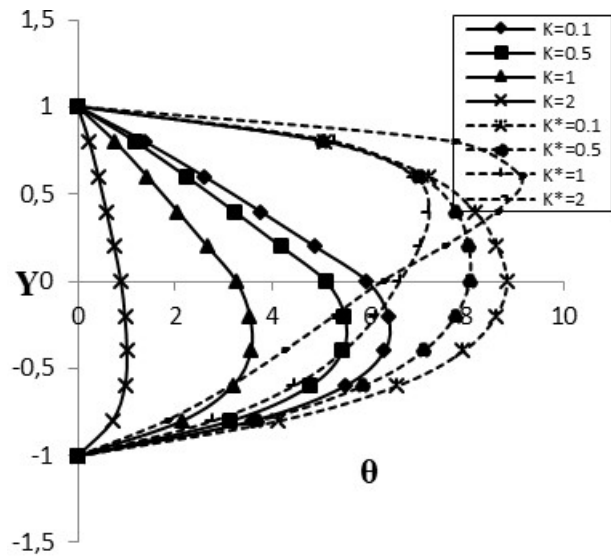


Fig.30. Temperature profiles θ_1, θ_2 (unsteady flow), θ_1^*, θ_2^* (steady flow) for various K and $M = 4, m = 2, \alpha = 0.333, h = 0.75, \beta = 1, \sigma_0 = 2, \sigma_1 = 1.2, \sigma_2 = 1.5, \epsilon = 0.5, \rho = 1, \omega = 1, t = \pi / \omega, s = 0.5$ (Conducting plates)

The effect of the viscosity ratio α on the velocity and temperature is depicted in Figs 31-33. Increasing α lowers the primary velocity distribution in region-I but reduces until the value reaches $\alpha = 0.9$, then grows in area II as illustrated in Fig.31. In Figure 32, we can see that in α decreases the secondary distribution in region-I, whereas it drops until $\alpha = 0.9$ in region-II, then grows. The temperature distribution in the two zones appears to be decreasing as it grows up to $\alpha = 0.333$, then increasing as seen in Fig.33. The temperature distribution in the channel tends to migrate below the channel centre line, towards region-II, as the channel temperature rises.

The effects of the height ratio h on the primary and secondary velocities and temperature are shown in Figs 34-36. Figure 34 indicates that increasing h boosts the primary velocity distribution up to $h = 0.5$, then diminishes but beyond $h = 1$ increases in the two zones. Figure 35 demonstrates that when the value of h increases, the secondary velocity distribution grows until it reaches $h = 0.75$, at which point it descends into region-I. In region-II, as h increases, the secondary velocity distribution grows, then drops as $h = 1$. The maximum primary and secondary velocity distributions of the channel tend to migrate below the channel

centre line, towards region-II, as h increases. When h is increased, the temperature distribution decreases until it reaches $h = 0.5$, at which point it increases in region-I and decreases in region-II. As h increases, the channels maximum temperature tends to fall below the channel centre line, towards region-II.

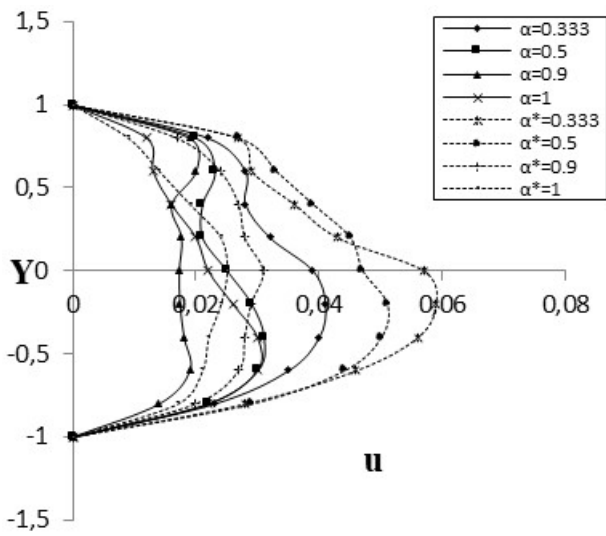


Fig.31. Primary velocity profiles u_1, u_2 (unsteady flow), u_1^*, u_2^* (steady flow) for various α and $M = 2, m = 2, h = 1, K = 2, \sigma_0 = 1, \sigma_1 = 1.2, \sigma_2 = 1.5, \epsilon = 0.5, \rho = 1, \omega = 1, t = \pi / \omega, s = 0.5$, (Conducting plates)

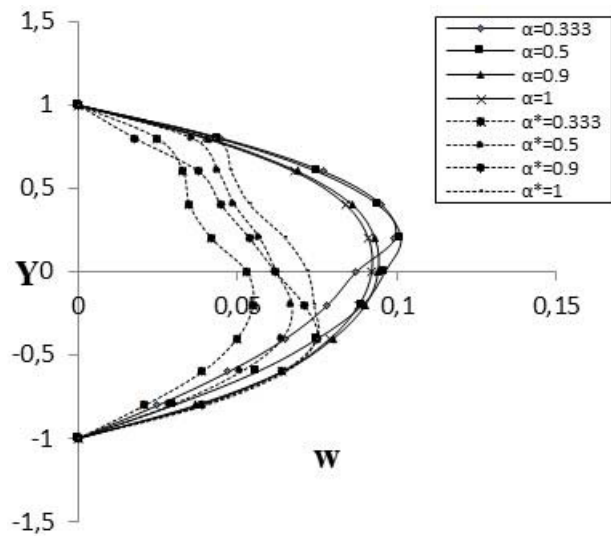


Fig.32. Secondary velocity profiles w_1, w_2 (unsteady flow), w_1^*, w_2^* (steady flow) for various α and $M = 2, m = 2, h = 1, K = 2, \sigma_0 = 1, \sigma_1 = 1.2, \sigma_2 = 1.5, \epsilon = 0.5, \rho = 1, \omega = 1, t = \pi / \omega, s = 0.5$, (Conducting plates)

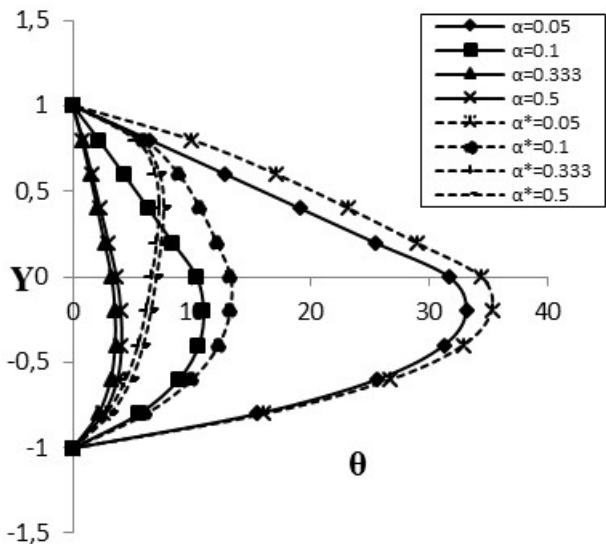


Fig.33. Temperature profiles θ_1, θ_2 (unsteady flow), θ_1^*, θ_2^* (steady flow) for various α and $M = 4, m = 2, h = 0.75, K = 1, \beta = 1, \sigma_0 = 2, \sigma_1 = 1.2, \sigma_2 = 1.5, \epsilon = 0.5, \rho = 1, \omega = 1, t = \pi / \omega, s = 0.5$ (Conducting plates)

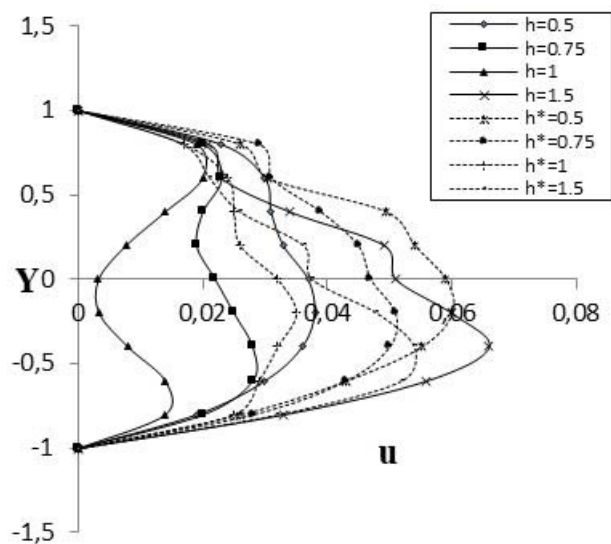


Fig.34. Primary velocity profiles u_1, u_2 (unsteady flow), u_1^*, u_2^* (steady flow) for various h and $M = 2, m = 2, \alpha = 0.9, K = 2, \sigma_0 = 1, \sigma_1 = 1.2, \sigma_2 = 1.5, \epsilon = 0.5, \rho = 1, \omega = 1, t = \pi / \omega, s = 0.5$, (Conducting plates)

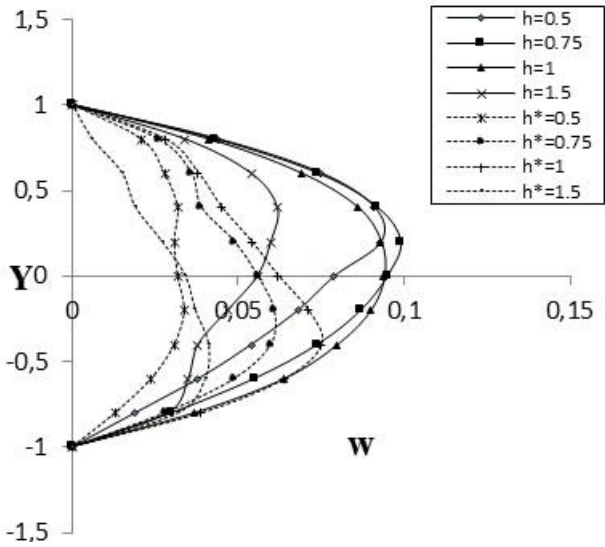


Fig.35. Secondary velocity profiles w_1, w_2 (unsteady flow), w_1^*, w_2^* (steady flow) for various h and $M = 2, m = 2, \alpha = 0.9, K = 2, \sigma_0 = 1, \sigma_1 = 1.2, \sigma_2 = 1.5, \epsilon = 0.5, \rho = 1, \omega = 1, t = \pi / \omega, s = 0.5$, (Conducting plates)

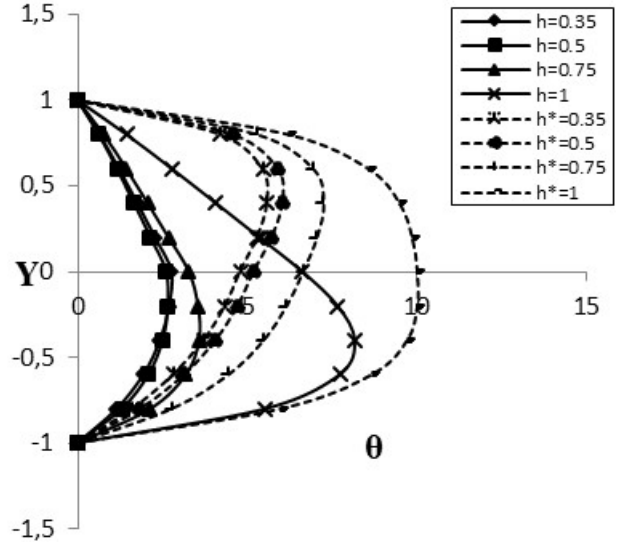


Fig.36. Temperature profiles θ_1, θ_2 (unsteady flow), θ_1^*, θ_2^* (steady flow) for various h and $M = 4, m = 2, \alpha = 0.333, \beta = 1, K = 1, \sigma_0 = 2, \sigma_1 = 1.2, \sigma_2 = 1.5, \epsilon = 0.5, \rho = 1, \omega = 1, t = \pi / \omega, s = 0.5$, (Conducting plates)

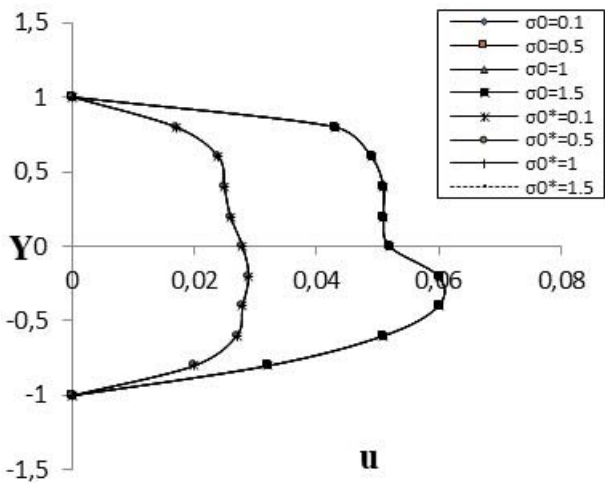


Fig.37. Primary velocity profiles u_1, u_2 (unsteady flow), u_1^*, u_2^* (steady flow) for various σ_0 and $M = 2, m = 2, \alpha = 0.9, h = 1, K = 2, \sigma_1 = 1.2, \sigma_2 = 1.5, \epsilon = 0.5, \rho = 1, \omega = 1, t = \pi / \omega, s = 0.5$, (Conducting plates)

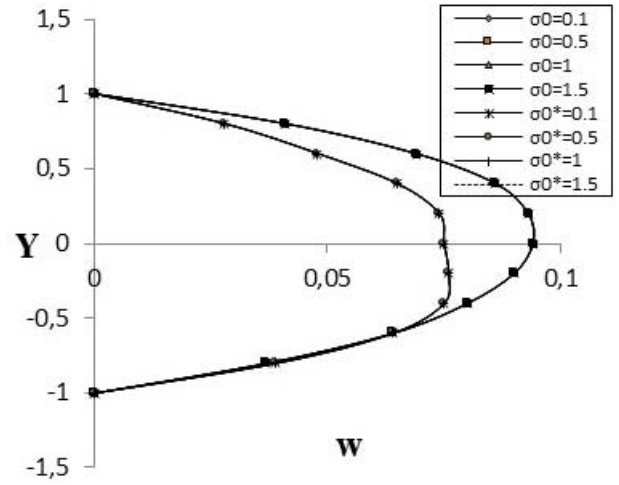


Fig.38. Secondary velocity profiles w_1, w_2 (unsteady flow), w_1^*, w_2^* (steady flow) for various σ_0 and $M = 2, m = 2, \alpha = 0.9, h = 1, K = 2, \sigma_1 = 1.2, \sigma_2 = 1.5, \epsilon = 0.5, \rho = 1, \omega = 1, t = \pi / \omega, s = 0.5$, (Conducting plates)

The electrical conductivity ratios influence is seen in Figs 37-39. The primary and secondary velocity distributions show no significant variation as σ_0 increases. The maximum primary and secondary velocity distributions of the channel tend to shift below the channel centre line, towards region-II, as the

value of σ_0 increases. The temperature distribution in the two zones increases as σ_0 rises. The maximum temperature tends to shift above the channel centre line, towards region-I, as σ_0 grows.

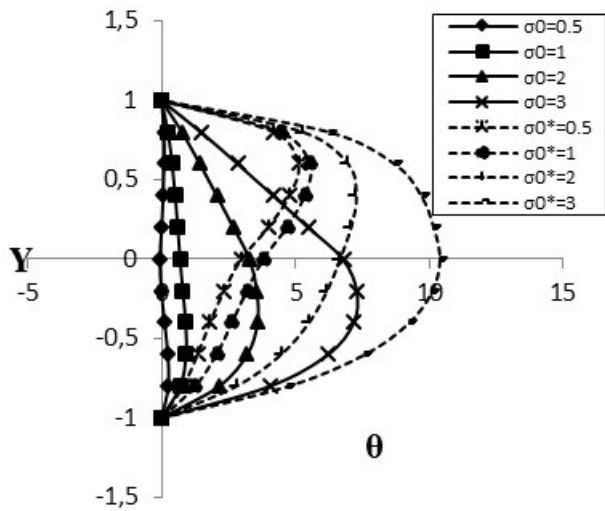


Fig.39. Temperature profiles θ_1, θ_2 (unsteady flow), θ_1^*, θ_2^* (steady flow) for various σ_0 and $M = 4$, $m = 2$, $\alpha = 0.333$, $h = 0.75$, $\beta = 1$, $\sigma_1 = 1.2$, $\sigma_2 = 1.5$, $K = 1$, $\epsilon = 0.5$, $\rho = 1$, $\omega = 1$, $t = \pi / \omega$, $s = 0.5$ (Conducting plates)

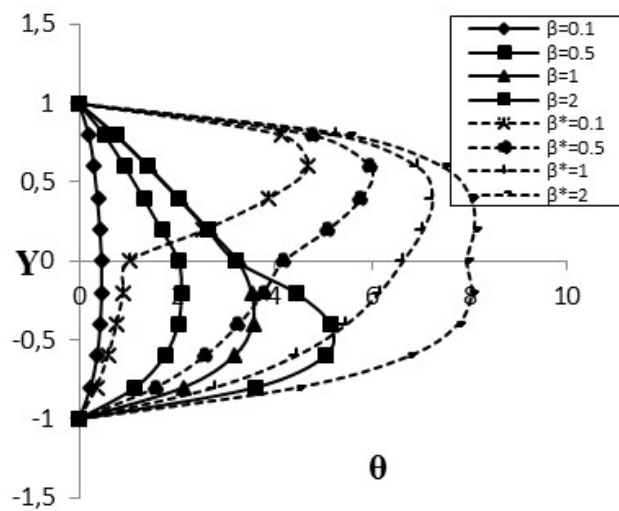


Fig.40. Temperature profiles θ_1, θ_2 (unsteady flow), θ_1^*, θ_2^* (steady flow) for various β and $M = 4$, $m = 2$, $\alpha = 0.333$, $h = 0.75$, $\sigma_0 = 2$, $\sigma_1 = 1.2$, $\sigma_2 = 1.5$, $K = 1$, $\epsilon = 0.5$, $\rho = 1$, $\omega = 1$, $t = \pi / \omega$, $s = 0.5$ (Conducting plates)

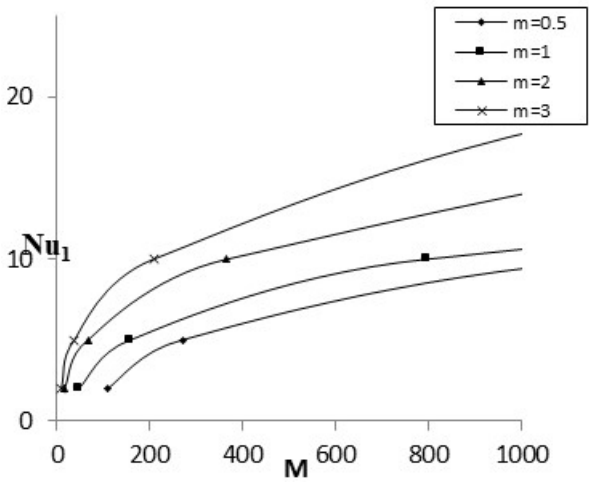


Fig.41. Nusselt Number Nu_1 for various M and $\alpha = 0.333$, $h = 0.75$, $\sigma_0 = 1$, $\sigma_1 = 1.2$, $\sigma_2 = 1.5$, $K = 1$, $\epsilon = 0.5$, $\rho = 1$, $\beta = 1$, $\omega = 1$, $t = \pi / \omega$, $s = 0.5$ (Conducting plates)

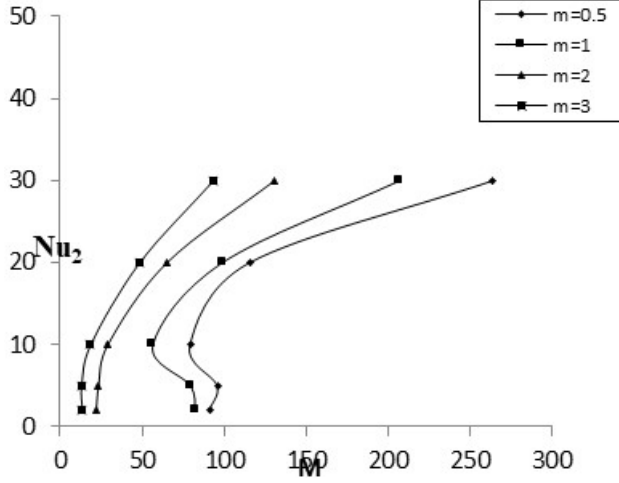


Fig.42. Nusselt Number Nu_2 for various M and $\alpha = 0.333$, $h = 0.75$, $\sigma_0 = 1$, $\sigma_1 = 1.2$, $\sigma_2 = 1.5$, $K = 1$, $\epsilon = 0.5$, $\rho = 1$, $\beta = 1$, $\omega = 1$, $t = \pi / \omega$, $s = 0.5$ (Conducting plates)

The thermal conductivity ratios effect on the temperature distribution is seen in Fig.40. Rising β raises the temperature distribution up to $\beta = 1$, after which the temperature distribution in region-I decreases

while the temperature distribution in region-II increases. The maximum temperature in the channel tends to fall somewhat below the channel centre line, towards region-II, as the value of β increases.

Figures 41 and 42 show the rate of heat transfer coefficient against the Hartmann number for various Hall parametric values m . Increases in either the Hartmann number or the Hall parameter increase the rate of heat transfer coefficient at the two plates, as seen in Figs 41 and 42.

In light of the foregoing points of discussion, it has been discovered that the controlling parameters such as the Hartmann number, Hall parameter, rotation parameter, thermal conductivity, and viscosity ratio have a significant impact on the flow and heat transfer factors, and thus the findings of this study may be applicable in a variety of engineering and industrial issues.

5. Conclusion

When the side plates of a rotating system are formed of a conducting material, the impact of Hall currents on MHD two liquid unsteady flows of plasma along a straight channel surrounded by infinitely long plates is investigated. The solutions for velocity and temperature fields in the 2-liquid zones are found to dependent on the electron pressure to total pressure ratio only. The effects of the Hartmann number, Hall parameter, rotation parameter, and viscosities, densities, heights, electrical conductivities, and thermal conductivities ratio on the velocity and temperature distributions in two liquid zones are investigated using distribution profiles for two different cases where the ionization parameter is either zero or half. The main research findings are summarized in the following points for two cases:

In the instance of electron-to-total pressure ratio $s = 0$:

- A raise in the Hartmann number decreases both the velocity and temperature.
- An increase in the Hall parameter diminishes the main flow and temperature while boosts the transverse velocity (secondary velocity component).
- A rise in the Taylor number lessens the main flow and temperature in both regions, whereas the transverse velocity grows up to a specific estimate and thereafter drops.
- A boost in the thermal conductivity ratio increases the temperature until it reaches a specific value after which it falls in region-I, while boosts in region-2.
- As the Hartmann number grows, the rate of heat transfer coefficient at the two plates increases.
- Increasing the Hall parameter up to a certain estimate lowers the rate of heat transfer coefficient at the upper plate and raises it beyond that estimate.
- As the Hall parameter increases, the rate of heat transfer coefficient increases at the lower plate.

Acknowledgements

The resources required to carry out this research were provided by my alma mater, "Andhra University" to which the authors would like to express their gratitude. The chief editor, Prof. Pawel Jurczak, is also to be thanked for his help in getting this study published and for his wise remarks.

Nomenclature

- $B_1, B_2, \dots, b_1, b_2, \dots$ – coefficients /notations used for simplicity in the main equations and solutions
 B_0 – applied uniform magnetic field
 c_{p_i} ($i = 1, 2$) – specific heat at constant pressure in the two-fluid region
 E_{ix}, E_{iz} , ($i = 1, 2$) – applied electric fields in the x - and z - directions, where $\vec{E}_i = (E_{ix}, 0, E_{iz})$
 h – ratio of the heights of the two regions
 h_1 – height of the channel in the upper region (region-I)
 h_2 – height of the channel in the lower region (region-II)
 I_{ix}, I_{iz} ($i = 1, 2$) – dimensionless current densities along x - and z - directions in region-I and region-II, that is, $I_{1x}, I_{1z}; I_{2x}, I_{2z}$

- I_1, I_2 ; – symbols for currents in two-fluids, where current density:
 $I_1 = I_{1x} + iI_{1z}$; $I_2 = I_{2x} + iI_{2z}$ $\bar{J}_i = (J_{ix}, 0, J_{iz})$, ($i = 1, 2$)
- J_{ix}, J_{iz} – current densities along the x- and z- directions in the two fluid regions
- K_1, K_2 – thermal conductivities of the two fluids
- $K = \sqrt{\frac{h_l^2 \rho \Omega}{\mu_l}}$ – Taylor number (rotation parameter)
- M – Hartman number $M = \sqrt{\sigma_{0l} B_0^2 h_l^2 / \mu_l}$
- m – Hall parameter where $m = \omega_e / \left(\frac{1}{\tau} + \frac{1}{\tau_e} \right)$
- m_{ix}, m_{iz} , ($i = 1, 2$) – dimensionless electric fields for two fluids as m_{1x}, m_{1z}, m_{2x} and m_{2z}
- M_1, M_2 – notations where $M_1 = m_{1x} + im_{1z}$, $M_2 = m_{2x} + im_{2z}$
- Nu_1, Nu_2 – rate of heat transfer coefficients at upper and lower plates
- p – pressure
- p_e – electron pressure
- P_{ri} ($i = 1, 2$) – Prandtl number of the two fluids
- P_1, P_2, P_3, P_4 – notations used for: $P_1 = 1 - \frac{sm^2}{1+m^2}$, $P_2 = -\frac{sm}{1+m^2}$, $P_3 = 1 - \left(1 - \frac{\sigma_0 \sigma_{0l}}{1+m^2} \right) s$, $P_4 = \frac{-\sigma_0 \sigma_{02} ms}{1+m^2}$
- $q_{01}, q_{02}, q_{11}, q_{12}$ – velocities in complex notation for steady and transient state in the two fluid regions:
 $q_{01} = u_{01} + iw_{01}$, $q_{11} = u_{11} + iw_{11}$, $q_{02} = u_{02} + iw_{02}$, $q_{12} = u_{12} + iw_{12}$
- $q_1(y, t), q_2(y, t)$ – solutions of velocity distributions for the two fluids in complex form:
 $q_1(y, t) = q_{01}(y) + \varepsilon \cos \omega t \cdot q_{11}(y)$, $q_2(y, t) = q_{02}(y) + \varepsilon \cos \omega t \cdot q_{12}(y)$
- $s = \frac{p_e}{p}$ – ionization parameter (ratio of electron pressure to the total pressure)
- t – time
- T_i ($i = 1, 2$): T_1, T_2 – temperatures of the fluids in region-I and region-II
- u_i , ($i = 1, 2$): u_1, u_2 – primary velocity distributions (velocity components along the x-direction)
in region-I and -II
- $u_{01}(y), u_{02}(y)$ – steady state primary velocities in the two fluid regions
- $u_{11}(y), u_{12}(y)$ – transient primary velocity components in the two fluid regions
- u_{1m}, u_{2m} – primary mean velocity distributions in the two fluid regions
- $u_p = \left(-h_l^2 / \mu_l \right) \frac{\partial p}{\partial x}$ characteristic velocity
- \bar{V}_i – fluid velocity
- w_i , ($i = 1, 2$): w_1, w_2 – secondary velocity distributions (component of velocity field along the z-direction)
in the two fluid regions
- $w_{01}(y), w_{02}(y)$ – steady state secondary velocity components in the two fluid regions
- $w_{11}(y), w_{12}(y)$ – transient secondary velocities in the two regions
- (x, y, z) – space co-ordinates in the rectangular Cartesian co-ordinate system
- $-\frac{\partial p}{\partial x}$ – common constant pressure gradient

Greek Symbols

- α – $= \mu_1 / \mu_2$, ratio of the viscosities
- β – $= \frac{K_1}{K_2}$, thermal conductivity ratio
- μ_i ($i = 1, 2$): μ_1, μ_2 – viscosities of the two fluids

- σ_{0i} ($i = 1, 2$), σ_{01} , σ_{02} – electrical conductivities of the two fluids
 σ_0 – ratio of electrical conductivities $\sigma_0 = \sigma_{01}/\sigma_{02}$
 σ_{11} , σ_{12} , σ_{21} , σ_{22} – modified conductivities parallel and normal to the direction of electric fields
 σ_1, σ_2 – symbols for the ratios $\sigma_1 = \sigma_{12}/\sigma_{11}$, $\sigma_2 = \sigma_{22}/\sigma_{21}$
 ρ_1, ρ_2 – densities of the two fluids
 ρ – $\frac{\rho_2}{\rho_1}$, density ratio of the two fluids
 θ_1, θ_2 – dimensionless temperature distributions for the two-fluid regions
 $\theta_{01}(y), \theta_{02}(y)$ – steady state temperature distributions in the two fluid regions
 $\theta_{11}(y), \theta_{12}(y)$ – transient temperature distributions in the two fluid regions
 τ, τ_e – mean collision time between electron and ion, electron and neutral particles
 ε – amplitude (a small constant quantity, $\varepsilon \ll 1$)
 ω – frequency of oscillation
 ω_e – gyration frequency of electron
 Ω – angular velocity, where $\vec{\Omega} = (0, \Omega, 0)$

Subscripts 1,2 – refers to the quantities in the upper and lower fluid regions: region-I and region-II

References

- [1] Blum Ya. E. (1967): *Heat and Mass Transfer in Magnetic Field.*– Magneto hydrodynamics, vol.11, No.1, pp.27-36.
- [2] Ryabinin A.G. and Khozhainov A.I. (1967): *Exact and approximate formulations of problems for unsteady flows of conducting fluids in MHD channels.*– Fluid Dyn., vol.2, No.4, pp.107-109. <https://doi.org/10.1007/BF01019553>
- [3] Cramer Kenneth R. and Pai Shih I. (1973): *Magneto Fluid Dynamics for Engineers and Applied Physicists.*– McGraw-Hill Company, New York.
- [4] Debnath L. (1975): *Inertial oscillations and hydro magnetic multiple boundary layers in a rotating fluid.*– ZAMM (Zeitschrift Fur AngewandteMathematik and Mechanik), vol.55, No.3, pp.141-147. <https://doi.org/10.1002/zamm.19750550303>
- [5] Mazumder B.S. (1977): *Effect of wall conductances on hydro magnetic flow and heat transfer in a rotating channel.*– ActaMechanica, vol.28, No.1, pp.85-99. <https://doi.org/10.1007/BF01208791>
- [6] Shercliff J.A.(1979):*Thermoelectric magneto hydrodynamics.*– J.Fluid Mechanics,vol.91, No.2, pp.231-251. DOI: <https://doi.org/10.1017/S0022112079000136>
- [7] Chen L., Gong J., Sun F. and Wu C. (2002): *Heat transfer effect on the performance of MHD power plant.*– Energy Conversion and Management, vol.43, No.15, pp.2085-2095.
- [8] Morley N.B., Malang S. and Kirillov I. (2005): *Thermo fluid magneto hydrodynamic issues for liquid breeders.*– Fusion Science and Technology, vol.47, pp.488-501
- [9] Hardianto T., Sakamoto N. and Harada N. (2008): *Computational study of diagonal channel magneto hydrodynamic power generation.*– Int. J. Energy Tech. Policy, vol.6, pp.96-111.
- [10] Soward A.M. and Dormy E. (2010): *Shear-layers in magneto hydrodynamic spherical Couette flow with conducting walls.*– Journal of Fluid Mechanics, vol.645, pp.145-185.
- [11] Seth G.S., Mahto N., Ansari S. and Nandkeolyar, R. (2010): *Combined free and forced convection flow in a rotating channel with arbitrary conducting walls.*– International Journal of Engineering, Science and Technology, vol.2, No.5, pp.184-197.
- [12] Kabeel A.E., Emad El-Said M.S. and Dafea S.A. (2015): *A review of magnetic fields effects on flow and heat transfer in liquids: Present status and future potential for studies and applications.*– Renewable and Sustainable Energy Reviews, vol.45, pp.830-837.

- [13] Das S., Jana R.N. and Makinde O.D. (2016): *Transient hydro magnetic reactive Couette flow and heat transfer in a rotating frame of reference.*– Alexandria Engg. Journal, vol.58, pp.635-644.
- [14] Sato H. (1961): *The Hall effect in the viscous flow of ionized gas between parallel plates under transverse magnetic field.*– J. Phys. Soc. Japan, vol.16, No.7, pp.1427-1433. <https://doi.org/10.1143/JPSJ.16.1427>
- [15] Tani I.(1962): *Steady flow of conducting fluids in channels under transverse magnetic fields, with consideration of Hall effect.*– Journal of the Aerospace Sciences, vol.29, No.3, pp.297-305.
- [16] Pop I. and Soundalgekar V.M. (1977): *The Hall effect on an unsteady flow due to a rotating infinite disc.*– Nuclear Engineering and Design, vol.44, No.3, pp.309-314.
- [17] Niranjana S.S., Soundalgekar V.M. and Takhar, H.S. (1990): *Free convection effects on MHD horizontal channel flow with Hall currents.*– Plasma Sci. IEEE Trans, vol.18, No.2, pp.177-183.
- [18] Linga Raju T. and Ramana Rao V.V. (1992): *Hall effect in the viscous flow of an ionized gas between two parallel walls under transverse magnetic field in a rotating system.*– Acta Physica Hungarica (Springer), vol.72, No.1, pp.23-45. <https://doi.org/10.1007/BF03177494>
- [19] Linga Raju T. and Ramana Rao V.V.(1993): *Hall effects on temperature distribution in a rotating ionized hydro magnetic flow between parallel walls.*– Int. J. Engg. Sci., vol.31, No.7, pp.1073-1091. [https://doi.org/10.1016/0020-7225\(93\)90115-B](https://doi.org/10.1016/0020-7225(93)90115-B)
- [20] Attia H.A. (1998): *Hall current effects on the velocity and temperature fields of an unsteady Hartmann flow.*– Can. J. Phys, vol.76, No.9, pp.739-746.
- [21] Ghosh S.K. and Pop I. (2004): *Hall effects on MHD plasma Couette flow in rotating environment.*– Int. J. Appl. Mech. and Engg, vol.9, pp.293-305.
- [22] Ghosh S.K., Beg O.A. and Narahari M. (2009): *Hall effects on MHD flow in a rotating system with heat transfer characteristics.*– Mecanica, vol.44, pp.741-765.
- [23] Jha B.K. and Apere C.A. (2010): *Combined effects of Hall and ion-slip currents on unsteady MHD Couette flows in a rotating system.*– J. Phys. Soc. Japan, vol.79. DOI:10.1143/JPSJ.79.104401.
- [24] Singh J.K., Begum S.G. and Seth G.S. (2018): *Influence of Hall current and wall conductivity on hydro magnetic mixed convective flow in a rotating Darcian channel.*– Physics of Fluids, vol.30, No.11, pp.113602-1 to 12.
- [25] Shail R. (1973): *On laminar two-phase flows in magneto hydrodynamics.*– Int. J. Engg. Sci., vol.11, pp.1103-1109. [https://doi.org/10.1016/0020-7225\(73\)90111-0](https://doi.org/10.1016/0020-7225(73)90111-0)
- [26] Chawla T.C. and Ishii M. (1980): *Two-Fluid model of two-phase flow in a pin bundle of a Nuclear Reactor.*– Int. J. Heat Mass Transfer, vol.23, No.7, pp.991-1001.
- [27] Lohrasbi J. and Sahai V. (1988): *Magneto hydrodynamic heat transfer in two phase flow Between parallel plates.*– Appl. Sci. Res. vol.45, pp.53-66.
- [28] Malashetty M.S. and Leela V. (1992): *Magneto hydrodynamic heat transfer in two phase flow.*– Int. J. of Engg. Sci. vol.30, No.3, pp.371-377. [https://doi.org/10.1016/0020-7225\(92\)90082-R](https://doi.org/10.1016/0020-7225(92)90082-R)
- [29] Chamkha A.J. (1995): *Hydro magnetic two-phase flow in a channel.*– Int. J. Engg. Sci., vol.33, No.3, pp.437-446. [https://doi.org/10.1016/0020-7225\(93\)E0006-Q](https://doi.org/10.1016/0020-7225(93)E0006-Q)
- [30] Hyun S. and Kennel C.F. (2009): *Small amplitude waves in a hot relativistic two-fluid plasma.*– J. Plasma Phy., vol.20, No.2, pp.281-287.
- [31] Linga Raju T. (2019): *MHD heat transfer two-ionized fluids flow between two parallel plates with Hall currents.*– Results in Engineering, vol.4, 100043, Elsevier BV, <http://doi.org/10.1016/j.rineng.2019.100043>.
- [32] Linga Raju T. (2021): *Electro-magneto hydrodynamic two fluid flow of ionized-gases with Hall and rotation effects.*– Int. J. Appl. Mech., vol.26, No.4, pp.128-144. DOI: 10.2478/ijame-2021-0054
- [33] Mitra P. (1982): *Unsteady flow of two electrically conducting fluids between two rigid parallel plates.*– Bulletin of the Calcutta Mathematical Society, vol.74, pp.87-95.
- [34] Hasnain Qaisrani M., ZhenWei Xia and Dandan Zou (2005): *Statistical properties of three-Dimensional two-fluid plasma model.*– Phys. Plasmas, vol.22, 092303, <https://doi.org/10.1063/1.4928900>
- [35] Umavathi J.C., Mateen A., Chamkha A.J. and Mudhaf A.A. (2006): *Oscillatory Hartmann two-fluid flow and heat transfer in a horizontal channel.*– Int. J. Appl. Mech. and Engg., vol.11, No.1, pp.155-178.

- [36] Linga Raju T. and Sreedhar S. (2009): *Unsteady two-fluid flow and heat transfer of conducting fluids in channels under transverse magnetic field.*– Int. J. Appl. Mech. and Engg., vol.14, No.4, pp.1093-1114.
- [37] Linga Raju T. and Nagavalli M. (2014): *MHD two-layered unsteady fluid flow and heat transfer through a horizontal channel between parallel plates in a rotating system.*– Int. J. Appl. Mech. and Engg., vol.19, No.1, pp.97-121.
- [38] Sharma P.R. and Sharma K. (2014): *Unsteady MHD two-fluid flow and heat transfer through a horizontal channel.*– Int. J. of Engineering Science Invention Research and Development, vol.1, No.3, pp.65-72.
- [39] Gireesha B.J., Mahantesh B., Thammanna G.T. and Sampathkumar P.B.(2018): *Hall effects on dusty nano-fluid two-phase transient flow past a stretching sheet using KVL model.*– Jour. of Molecular Liquids, vol.256, pp.139-147, <https://doi.org/10.1016/j.molliq.2018.01.186>
- [40] Sivakamini L and Govindarajan A. (2019): *Unsteady MHD flow of two immiscible fluids under chemical reaction in a horizontal channel.*– AIP conference proceedings 2112, 020157, <https://doi.org/10.1063/1.5112342>, published online: 24 June 2019.
- [41] AbdElmaboud Y, Abdesalam Sara I, Mekheimer Kh.S. and Kambiz Vafai (2019): *Electromagnetic flow for two-layer immiscible fluids.*– Engineering Science and Technology an International Journal, vol.22, pp.237-248, <https://doi.org/10.1016/j.jestch.2018.07.018>
- [42] Linga Raju T. and GowriSankara Rao V. (2021): *Effect of Hall current on unsteady magneto hydro dynamic two-ionized fluid flow and heat transfer in a channel.*– Int. J. of Applied Mechanics and Engg., vol.26, No. 2, pp.84-106, DOI: 10.2478/ijame-2021-0021
- [43] Linga Raju T. and Venkat Rao B.(2022): *Unsteady electro-magneto hydrodynamic flow and heat transfer of two ionized fluids in a rotating system with Hall currents.*– Int. J. Appl. Mech., vol.27, No.1, pp.125-145.

Received: February 26, 2022

Revised: June 28, 2022